Chapter 9
Nanomaterials for the Photoremediation of Pollutants

Mohammad Chahkandi and Mahboobeh Zargazi

Contents

Abstract The restricted global fear within contaminated ecosystem has been motivated the impress works to employ the photocatalytic degradation of organic pollutants and pesticides. Generally, stability and water solubility of pesticides cause high impacts on environment due to high resistance in ecosystem. Heterogeneous nano-photocatalyst can be introduced as one of the most appealing technologies bearing great remediation performance because of the high surface area and intense correlated activity. The heterogeneous catalytic nanomaterials have been operated to

M. Chahkandi (✉)
Department of Chemistry, Hakim Sabzevari University, Sabzevar, Iran
e-mail: m.chahkandi@hsu.ac.ir

M. Zargazi
Department of Chemistry, Faculty of Science, Ferdowsi University of Mashhad, Mashhad, Iran

Inamuddin et al. (eds.), *Water Pollution and Remediation: Photocatalysis*, Environmental Chemistry for a Sustainable World 57,
https://doi.org/10.1007/978-3-030-54723-3_9

harvest, turn, and supply clean and renewable sunlight energy. It can be performed through entire water splitting and CO production to provide green-sustainable solar fuels alongside of wide ranges of environmental aspects. We reviewed in the presented chapter focusing on the application of effective nanomaterials in environmental remediation about industrial and agricultural effluents. For years TiO_2 photocatalyst has been largely utilized but includes restricted activity just in UV spectrum due to wide band gap. Therefore, it is crucial to development of new effective visible light-sensitive photocatalysts with lower band gap that can be activated by a notable percentage of the solar irradiations. Herein, we try to discuss the basic science drives for performance improving of visible/solar light photocatalysts. First, the corresponding principles which include of thermodynamics, kinetics, and recombination rate are followed. The second section reviews the new effective reported visible-activated photocatalytic compounds considering with proposed photoexcitation mechanisms and reducing the charges recombination. Finally, the main challenges and future prospects for better handling of photocatalytic technology were briefly discussed.

Keywords Nano-photocatalyst · Photocatalytic mechanism · UV-activated · Visible-activated · Semiconductor

9.1 Introduction

9.1.1 General Views of Photocatalytic Remediation

During the past centuries, increasing human energy demands have been resolved by fossil combustion-based sources such as oil, coal, and natural gases. The used sources caused different overproductions with known and unknown impacts on environment. Awareness about some other mineral fuel energies like nuclear source are insufficient from waste access and defect of technology points of view (Da Rosa 2012). However, the main adverse effects of mineral fuels on air, water, and soil can be regarded as global warming or impact on climate. Therefore, economic and population growing global societies have urgently asked for new, renewable, inexpensive, and easy affordable clean energy sources (Nuraje et al. 2012; Da Rosa 2012; Asmatulu 2015). The clean energy sources can be mainly achieved from natural sunlight, tides, wind, rain, biomass, and other sources without damaging the earth. The greatest and clean sun energy source has huge magnitude releasing near to 105 terawatts versus world's current energy requirement of 12 terawatts, 0.01% of total amount. Nanotechnology as ongoing technology can suggest approaches to degrading production charges, improving efficiency, and stashing energy, healthy environmental remediation, and so on (Asmatulu et al. 2010, 2011; Luque and Balu 2013; Nuraje et al. 2013). Obviously, industrialization have picked up greenhouse gas emission and particulate dust pollutants, continued over

Table 9.1 Advances oxidation processes for environmental remediation

Type of degradation technology	Example	References
Non-photochemical degradation	Sonochemical	Ghows and Entezari (2013)
	Electrochemical	Li et al. (2007)
	Fenton method (Fenton, electro-Fenton, Sono-Fenton)	Homem and Santos (2011) and Zhang et al. (2019)
	H_2O_2 oxidation	Bokare and Choi (2014)
	Supercritical water oxidation	Yao et al. (2018)
	Solvated electron reduction	Yu et al. (2018)
	Enzymatic treatment	Ahmed et al. (2017)
	Ozonation	Yang et al. (2018)
	O_3/H_2O_2	
	O_3/Catalyst	
Photochemical degradation	O_3/UV	Homem and Santos (2011)
	$O_3/UV/H_2O_2$	Rivera-Utrilla et al. (2013)
	Photo-Fenton, Photo- Fenton-electro, photo-Sono-Fenton	Barrera-Salgado et al. (2016) and Zhao et al. (2017)
	Photo-activated catalytic oxidation by UV/Visible	Chen et al. (2016) and Opoku et al. (2017)

the decades. Alternative route can be addressed by nanomaterials with photocatalytic degradation ability of greenhouse gases and other emission pollutants (Taherzadeh et al. 2013).

Environmental remediation can be performed by different methodologies, and that one of the widely used is chemical degradation. It can be achieved by different methods such as (1) photocatalytic, (2) Fenton method, (3) ozone/UV radiation/H_2O_2 oxidation, (4) sonochemical, (5) electrochemical, (6) supercritical water oxidation, (7) solvated electron reduction, (8) enzymatic treatment, and (9) the electron beam irradiation (Table 9.1) (Andreozzi et al. 1996, 1999; Jayaweera 2003; Gogate and Pandit 2004a, b; Babuponnusami and Muthukumar 2014). UV light and ozone alone have disinfection applications. The combined $O_3/UV/H_2O_2$ method progresses through oxidation/photolysis reactions, and generation of free hydroxyl radicals can highly degrade the organic pollutants. However, the secondary treatment for complete neutralization of pollutants should be executed through advanced oxidation processes. Advanced oxidation processes are achieved by complete mineralization of matters to H_2O and CO_2 through in fold of strong vibrant hydroxyl and superoxide radicals. Some of the most prevalent advanced oxidation processing technologies are listed in Table 9.1. One of the effective photodegradation reactions can be progressed using nano-semiconductor and solvated O_2 gas to form the promoter radicals. The principles of photocatalysis process of titania substrates were investigated based on "Honda–Fujishima effect" relating to photoinduced water splitting (Fujishima et al. 2008). Heterogeneous photocatalysts introduce efficient advanced oxidation processes within abatement of chemical pollutions. Advanced oxidation processes are associated with advantages of visible/white light-sensitive

photocatalysts having wide range of absorption spectra from UV to visible wavelengths (Herrmann 1995).

9.1.2 Photo-Effective Nanostructures

The binary and ternary metal oxides are initial photoactive particles used in photocatalytic structural devices such as solar cell, photoremediation, and water splitting. In order of environmental concerns, green, easygoing, and safe-producing methods of nanomaterials are fruitful. The desired techniques should include low temperature and high progress rate, with lowered hazardous agents or by-products. For example, one of the best photocatalysts, TiO_2, is generally synthesized by polymerizable complex approach, sol–gel reaction, and solid-state progress. However, the two first ones offer applicable performance than the last one because of providing small crystallite and particle size and controllable particle shape (Nuraje et al. 2012). Pure TiO_2 photocatalysts have not enough power to hydrogen production through water splitting. Therefore, some modification is needed such as loaded Pt or other metal ions to approach band gap of 3.2 eV or lower activated under UV light (Nuraje et al. 2012; Luque and Balu 2013; Asmatulu 2015). Despite above, ZrO_2 having high 5.0 eV band gap as an UV photocatalyst can split water without assisting of any co-catalyst. Photo-UV catalytic ability of ZrO_2 decreased by loading co-catalysts such as Pt, Au, and RuO_2. In the next sections, the base interaction of photon and photocatalysts, the mechanism, and thermodynamic aspects have been discussed. In the following, different kinds of UV-visible-activated catalysts have been investigated, in details.

9.2 Principles of Photocatalytic Progress

9.2.1 Sunlight Interactions

Green photo-induced nanostructures are considered due to its applicability for sustained energy generation and environmental remediation strategies through interactions with infinite sunlight irradiations. Nanoscale structures with great ratio of surface area to volume resulted in highly increase of sunlight interactions compared to bulk format of materials. Nanostructures can be suggested as ideal entrant for a broad diversity of environmental issues grounded on photocatalysis and photosynthesis (Frank et al. 2004; Kay et al. 2006; Verma et al. 2011; Spinelli et al. 2012; Beard et al. 2014; Yeo et al. 2014). Among whole releasing sun energy, only a few small portion is absorbed by the earth. Therefore, the important photosynthesis reactions are proceedings that can influence on human life as cultivation and forestry. Sunlight as continuous light spectrum includes from high wavelengths of radio to low ones of X, and gamma ray ranges in $1–10^{-13}$ m of wavelength

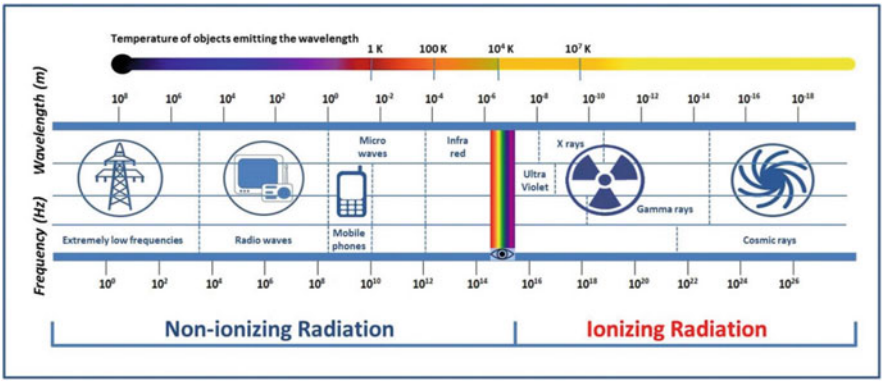

Fig. 9.1 Spectrum of electromagnetic waves. Sunlight as continuous light spectrum includes from high wavelengths of radio to low ones of X, and gamma rays range in $1–10^{-13}$ m of wavelength. (Saliev et al. 2019)

(Fig. 9.1). The small division of visible wavelengths from violet to red lights is considered in interaction of photocatalyst and visible light.

Actually, the passed sunlight from atmosphere of the earth interacts with photoactive materials in three ways: reflection, scattering, and absorption. Reflection specified as the fraction of reflected energy calls the reflectivity, R:

$$R = \frac{n_1 - n_2}{n_1 + n_2} \tag{9.1}$$

where n_1 and n_2 are refractive indices of two interface sides of the materials. Refractive index is explained as the ratio of light speed in vacuum against material. Scattering is defined as light orientation changing in randomly manner during the interaction to media that is divided to elastic and inelastic scattering kinds. Absorption happens when energy value of the light adapts the transition energy of the electrons of materials. In clear expression, absorption by an isolated material-bearing electronic density leads to the charge transition of the valence band across the band gap to the conduction band (Neil and Ashcroft 2016). For every transferred electron to conduction band, an unoccupied hole in valence band generates a pair known as e^-–h^+. It must be rephrased that absorption as the basic step of photocatalytic process is necessary for often applications of solar energy (Fig. 9.2).

9.2.2 Mechanistic View

There are 5–main steps involving the heterogeneous photocatalyst occurred from bulk of media toward to the final yield include of surface adsorption, photodegradation reactions, and desorption of conclusive products over the surface to the bulk media (see Fig. 9.3).

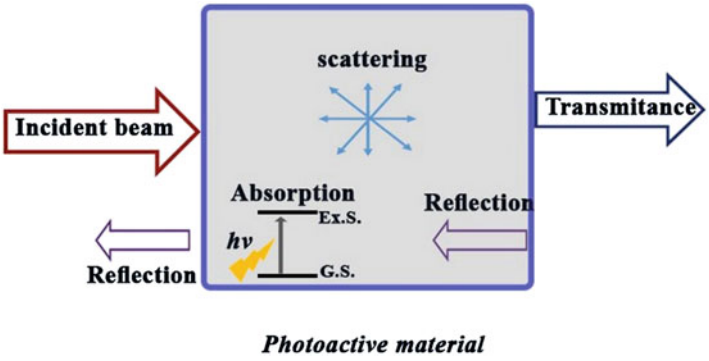

Fig. 9.2 Three ways of interaction of light with the material including reflection, scattering, and absorption. Ex. S. and G. S. represent excitation and ground states, respectively

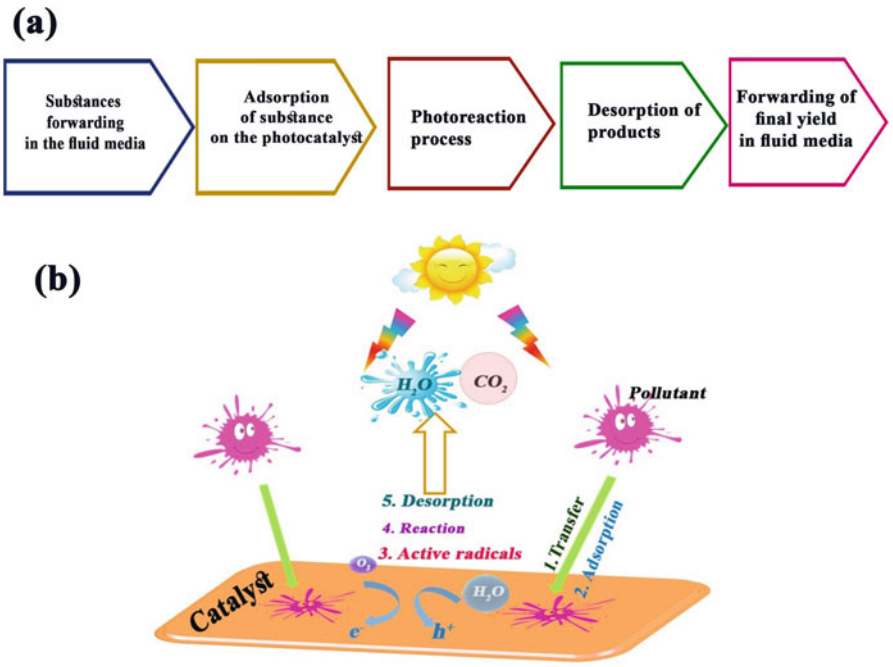

Fig. 9.3 Five possible main steps for interaction of light to the bulk of media and surface of the heterogeneous photocatalyst include surface adsorption, photodegradation reactions, and desorption of conclusive products over the surface to the bulk media

The basic photocatalytic reactions can be explained with six equations (see Fig. 9.4). The absorption of higher-energy photons versus the energy level of photocatalyst band gap is an essential primer step. Equation 9.2: Photon absorption leads to transfer of valence band electrons to conduction band and creation of hole

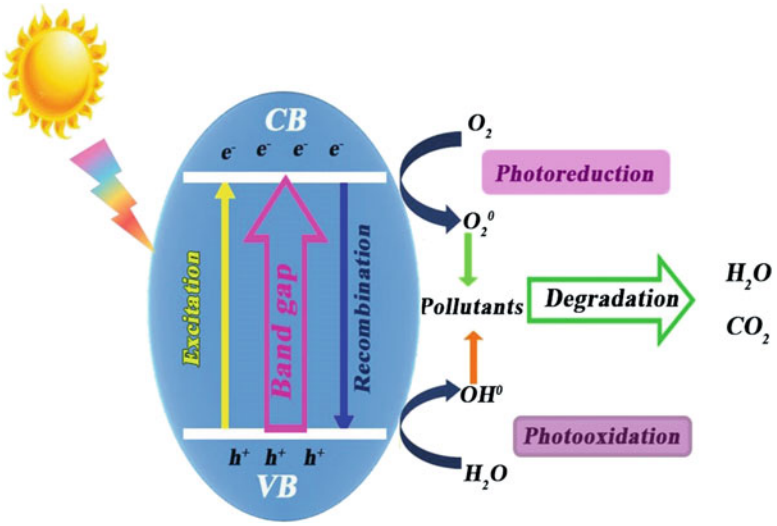

Fig. 9.4 The basic photocatalytic reactions can be explained with six equations: absorption of higher energy photons; transfer of valence band electrons to conduction band; recombination of existing electrons and holes and liberation of heat energy; reaction of produced electrons and involved oxidants; and reaction of holes and reductants. CB and VB stand for conductive band and valence band, respectively

over the valence band. Equation 9.3: The recombination of existing electrons and holes and liberation of energy in heat form is possible. Equations 9.4 and 9.5: Probable reaction of produced electrons and involved oxidants and also reaction of holes and reductants, to build vibrant radicals. Equations 9.6 and 9.7: The following shows degradation of pollution substances to mineralized carbon dioxide and water:

$$\text{Photocatalyst} + \text{energy} \rightarrow h^{+}_{\text{VB}} + e^{-}_{\text{CB}} \tag{9.2}$$

$$h^{+}_{\text{VB}} + e^{-}_{\text{CB}} \rightarrow \text{heat} \tag{9.3}$$

$$h^{+}_{\text{VB}} + \text{H}_2\text{O}\,(\text{Red}^{-}) \rightarrow {}^{\cdot}\text{OH} + \text{H}^{+} \tag{9.4}$$

$$e^{-}_{\text{CB}} + \text{O}_2(\text{Ox}^{+}) \rightarrow {}^{\cdot}\text{O}_2^{-}\,(\text{Superoxide radical}) \tag{9.5}$$

$${}^{\cdot}\text{OH} + \text{Contaminant} \rightarrow \text{Intermediates} \rightarrow \text{H}_2\text{O} + \text{CO}_2 \tag{9.6}$$

$${}^{\cdot}\text{O}_2^{-} + \text{Contaminant} \rightarrow \text{Intermediates} \rightarrow \text{H}_2\text{O} + \text{CO}_2 \tag{9.7}$$

9.2.3 Thermodynamic

The efficiency of catalytic process can be measured by two numeric and energetic methods. The numeric method needs to "inherent quantum efficiency; Ø" definition which means the products value ratio, based on primer photoreaction rate, and to value absorbed photons by system. In practical, in heterogeneous photocatalytic system, a mathematical term named "apparent quantum efficiency; ξ" is described as the ratio of reaction rate to the intensity of monochromatic light for concentration of i species C_i:

$$\xi_{C_i} = \pm(\mathrm{d}[C_i]/\mathrm{d}t)_0 / \left(\mathrm{d}[h\upsilon]_{\mathrm{int}}/\mathrm{d}t\right) \tag{9.8}$$

where $\pm(\mathrm{d}[C_i]/\mathrm{d}t)_0$ is change of initial rate of species concentration and $(\mathrm{d}[h\upsilon]_{\mathrm{int}}/\mathrm{d}t)$ is change of incident photo rate (Hoffmann et al. 1995).

Efficiency of energy conversion, ϵ, can be evaluated by ξ product to the changes ratio of Gibb's free energy to effective photon energy, E_p (Ohtani 2010):

$$\epsilon = \xi.\left(\Delta G/E_p\right) \tag{9.9}$$

The accurate value of recombination rate of hole and electron cannot be measured by the inherent quantum efficiency.

9.2.4 Kinetics of Catalytic Reactions

The reaction rate of general form of Eqs. 9.6 and 9.7 as $A + B \rightarrow C + D$ is given by:

$$r = -\mathrm{d}C_A/\mathrm{d}t = k\, C_A CB \tag{9.10}$$

where C_A, conduction band, and k are concentrations of A, B, and constant of reaction rate, respectively.

As illustrated in Fig. 9.3, heterogeneous photocatalytic process includes adsorption–desorption and reaction over the surface. It can be supposed that adsorption and desorption of reactants over the surface of catalyst is rapid. However, photocatalytic reaction is obviously the slowest step considered as the rate-determining step generally followed by Langmuir–Hinshelwood or L−H model. It should be formulated as:

$$r = -\mathrm{d}[\mathrm{Red}]/\mathrm{d}t = -\mathrm{d}[\mathrm{Ox}]/\mathrm{d}t = k\theta_{\mathrm{Red}}\theta_{\mathrm{Ox}} \tag{9.11}$$

where θ_{Red} means fraction of adsorbed reductant over the catalyst surface and θ_{Ox} means fraction of adsorbed oxidant over the catalyst surface.

Moreover, θ_i can be defined based on K_i, adsorption constant:

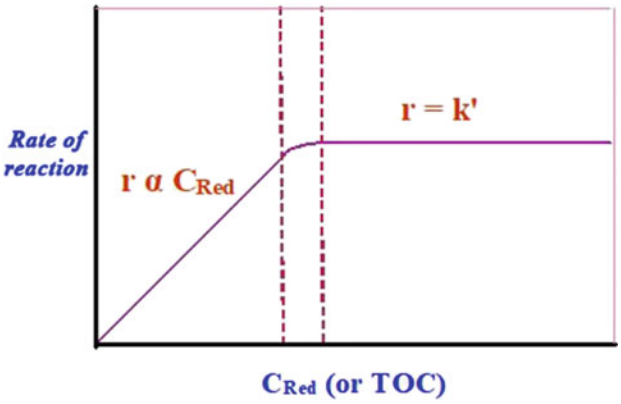

Fig. 9.5 The degradation rates at low concentrations of reductant conforms to first-order kinetics while independent at higher concentrations. C_{Red} stands for concentration of reduction

$$\theta_i = K_i C_i/(K_i C_i + 1) \tag{9.12}$$

Combination of Eqs. (9.11) and (9.12) can be rephrased as:

$$r = kK_{Red}C_{Red}K_{Ox}C_{Ox}/(K_{Red}C_{Red} + 1)(K_{Ox}C_{Ox} + 1) \tag{9.13}$$

Actually, K_i value which is experimentally determined in dark means no photocatalytic reaction. Some simple approximations can reduce the complexity form of Eq. (9.13). The oxidant can be considered as a pure liquid, so $\theta_{Ox} = 1$; or as a fluid solution, based on Henry's law, $\theta_{Ox} =$ constant. Therefore:

$$r = k'\theta_{Red} = k'K_{Red}C_{Red}/(K_{Red}C_{Red} + 1) \tag{9.14}$$

$$\begin{aligned} &\text{If } C_{Red} = C_{Red,\,max}\text{, so } \theta_{Red} = 1 \text{ and } r = k'. \\ &\text{In contrast, if } C_{Red} \ll C_{Red,\,max}\text{, so } \theta_{Red} = K_{Red}C_{Red} \\ &\quad \text{and } r = k'K_{Red}C_{Red} = K_{apparent}C_{Red} \end{aligned} \tag{9.15}$$

Therefore, the degradation rates at low concentrations of reductant conform to first-order kinetics while independent at higher concentrations (Fig. 9.5).

For overall rate estimation as complementary consideration, photomineralization rate of produced intermediates through Eqs. (9.6) and (9.7) can be stated based on total organic carbon; TOC or chemical oxygen demand; COD values (Minero et al. 1996; Malato et al. 2009):

$$r_{TOC,0} = \beta_1[\text{TOC}]/(\beta_2 + \beta_3[\text{TOC}]) \tag{9.16}$$

that $[\text{TOC}]_0$ is considered as the prime content of TOC at zero time, $t = 0$.

9.3 The Mechanistic Aspects of Visible/Sunlight Photoactivity

As aforementioned notes, a semiconductor photocatalyst absorbs the energetic photons that lead to the generation of electron–hole pairs with electron photoexcitation through heavy valence band to empty conduction band. As we know, very quick recombination of the generated electron–hole give rise to energy destruction and diminishing of quantum efficiency. Accordingly, novel-improving mechanisms for spare recombination are constantly pursued. The key issue for spare recombination is to stretch the photo-absorption region along with separation performance of electron–hole pairs. Producing of heterojunction kind of crystalline semiconductors is proposed as an operational solution. The effectiveness of a semiconductor within photocatalytic behavior crucially belongs to the energy alignment of the band gap. Interfaces of semiconductor heterojunction can be categorized into three types: straddling gap, type I; staggered gap, type II; and broken gap, type III (Fig. 9.6a). The great improvement can be achieved by conversion of traditional type II into direct Z- and S-schemes. S-scheme is built up as a combination of two n-type semiconductor photocatalysts. (Di et al. 2017; Low et al. 2017; Zhu et al. 2017; Fu et al. 2018, 2019; Tan et al. 2018; Li et al. 2019e) (Fig. 9.6b).

The effective developed photocatalysts can be categorized in four main classes: metal oxides (Zhu et al. 2017; Tan et al. 2018; Li et al. 2019e), sulfides (Tada et al. 2011; Zhang et al. 2012, 2016; Bai et al. 2013; Wei et al. 2018b), valuable metal semiconductors (Miao et al. 2013; Cai et al. 2017; Li et al. 2018a; Zhang et al. 2018b), and non-metallic semiconductors (Feng et al. 2018; Wu et al. 2018; Zheng et al. 2018; Qi et al. 2019; Reddy et al. 2019; Wang et al. 2019b). However, each photocatalyst has some disutility such as heavy metal or harmful leaching pollution, expensive, high thermal treatment, and low stability within catalytic reactions. Wang et al. (2008) reported that an applicable synthesized organic conjugated photocatalyst, named graphite carbon nitride (g-C_3N_4), has the capability of visible light absorption with band gap = 2.7 eV and $\lambda > 420$ nm for water splitting. g-C_3N_4 has various advantages such as easy preparation route, high stability, low cost, and visible frequencies sensitivity (Nayak et al. 2015; Jiang et al. 2018a; Li et al. 2019d; Xu et al. 2019b; Zhu et al. 2019). Therefore, recently huge attentions have been grown for preparation of pure g-C_3N_4 (Ma et al. 2018; Wang et al. 2018; Zhao et al. 2018), elemental loading modification (Wang et al. 2017; Bellardita et al. 2018; Da Silva et al. 2018; Deng et al. 2018; Shanker et al. 2018), heterogeneous composites (Tian et al. 2013; Zhou et al. 2014; Ran et al. 2018a), and diverse morphology preparation (Yang et al. 2015; Yu et al. 2016; Shakeel et al. 2019). The notable issue has many defects which exist with pure bulk g-C_3N_4 including small specific surface area (Sun and Liang 2017; Jiang et al. 2018b), low performance in solar irradiation ranges due to low absorption of wavelengths longer than 460 nm (Ye et al. 2015; Naseri et al. 2017; Shen et al. 2018; Zhang et al. 2018a), difficult film forming, and rapid electron–hole recombination (Hao et al. 2018; Jin et al. 2018; Shi et al. 2018) (see Fig. 9.7). Therefore, new composite compounds with specific morphology can

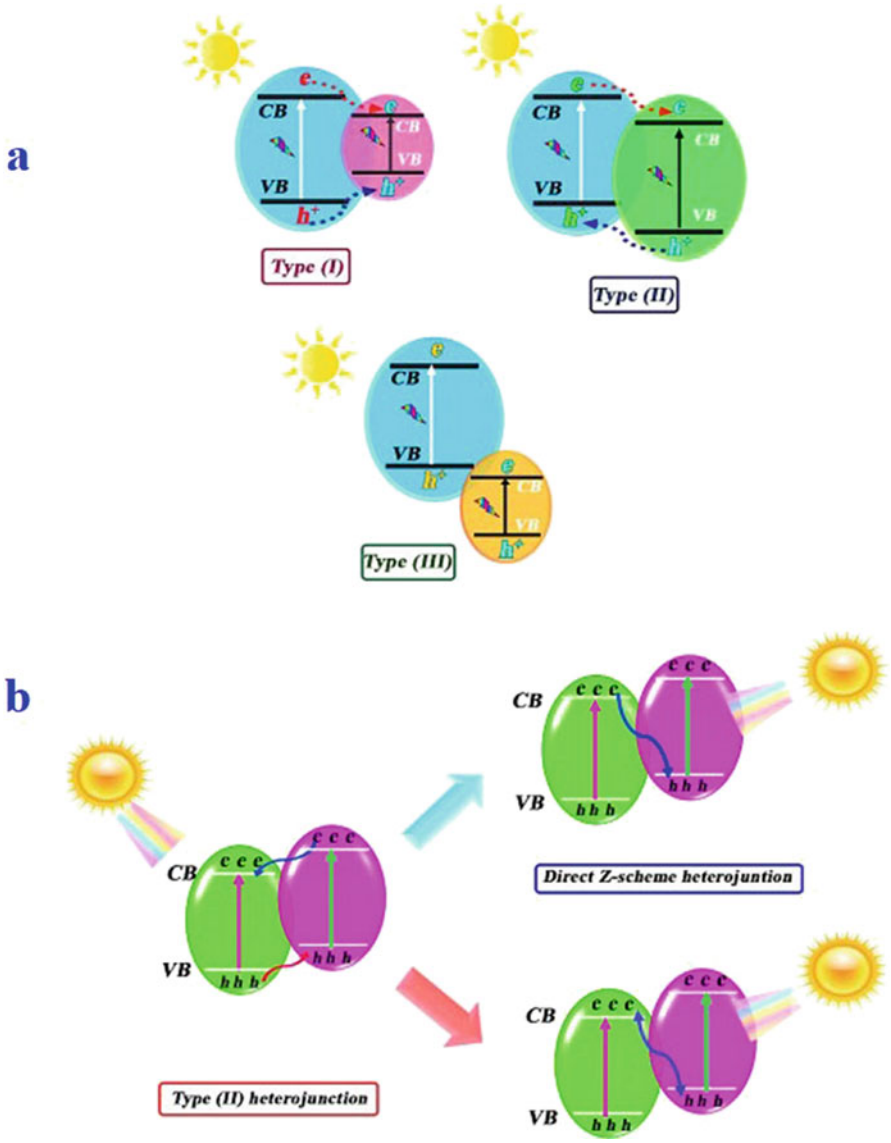

Fig. 9.6 (**a**) Three categories of interfaces of semiconductor heterojunction: straddling gap, type I; staggered gap, type II; and broken gap, type III. (**b**) The great improvement by conversion of traditional type II into direct *Z*- and *S*-schemes. CB and VB stand for conductive band and valence band, respectively

enhance photocatalytic efficiency (Li et al. 2015b, 2017c; Ong et al. 2016) using improved synthetic methods (Che et al. 2017; Li et al. 2017b), design of electronical structure (Ran et al. 2018b; Wei et al. 2018a; Wu et al. 2019), and nanostructure

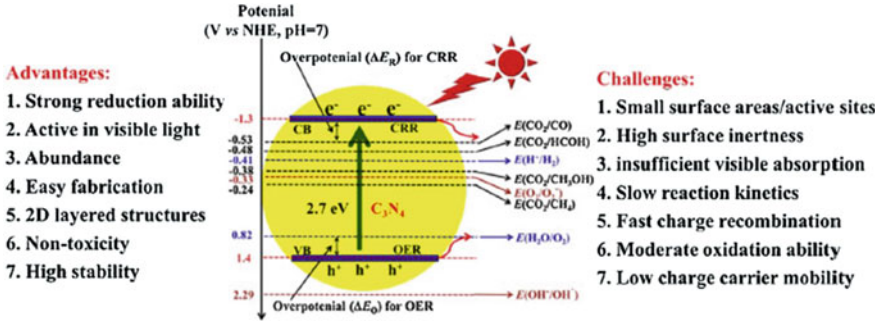

Fig. 9.7 The band gap influencing for redox potential of the appropriate reactions of g-C_3N_4 band edges at pH = 7. (Reprinted with permission of Elsevier from Wen et al. 2017)

manipulation (Dong et al. 2017; Ma et al. 2017; Li et al. 2018b). However, increasing researches about new composite materials of g-C_3N_4 highlight the potentially photocatalytic ability (Li et al. 2019c).

9.3.1 Heterogeneous Coupling

In order to inhibit recombination of formed electron and hole, achieving different surfaces of composited catalyst can be an approach. Therefore, heterostructured catalysts having various potentials of conduction bands and valence bands can be prepared. Through coupling construction, the excited electrons of conduction band having higher energy can move to the coupled catalyst conduction band. Analogously, electrons of valence band state of photocatalyst having higher potential should be excited to the valence band state of the coupled catalyst with lower-energy state (see Fig. 9.8). The progress is equivalent to the hole transferring of valence band with lower potential to the valence band of coupled one having higher potential state. Therefore, recombination rate will be reduced with transferring of generated electron–hole pairs to different surfaces of new coupled photocatalysts, resulting in improving photocatalytic efficiency.

UV-Activated Catalysts

Binary Metal Oxides

The binary metal oxides have mainly metal ions with d^0 configuration, which valence band and conduction band are combined of O 2p orbitals and d metal ones. The general examples are bimetallic TiO_2, Nb_2O_5, ZrO_2, Ta_2O_5, and WO_3, the anatase phase of the first one with lower band gap energy of 3.2 eV, determined as water splitting photocatalyst under UV irradiation. In order of effective photon

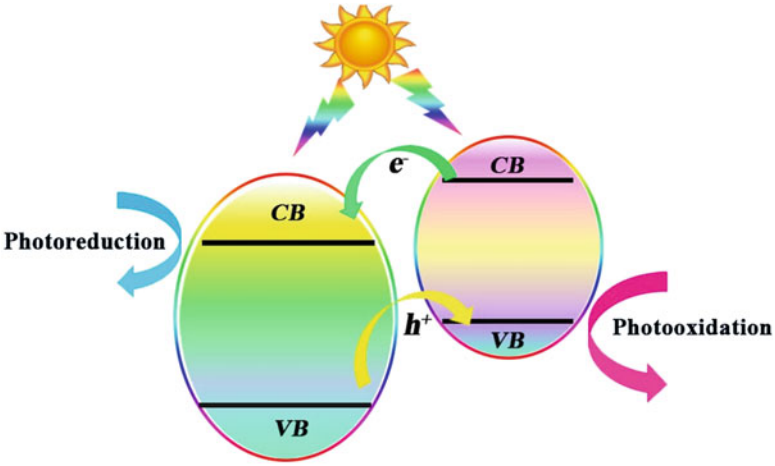

Fig. 9.8 Heterogeneous coupling leads to transfer of photo-prepared electrons and holes between surfaces of coupled photocatalysts and thus inhibition of recombination. CB and VB stand for conductive band and valence band, respectively

absorption of UV range, the band energy gap of photocatalyst should be lower than the UV energy light. The metal oxide having lesser energy of band gap must be reconstructed using cocrystal additives for proper water molecules splitting. TiO_2 with particles loading of Pt, RuO_2, NaOH, and Na_2CO_3 into photo-cocrystal TiO_2/Pt raises the water splitting activity (Duonghong et al. 1981; Akihiko et al. 1987). Moreover, coupling of TiO_2 with some second semiconductors of metal oxides such as SnO_2, Ag_xO, and ZrO_2 improves the photocatalytic efficiency. Therefore, the useful formed of heterostructures have higher photocatalytic ability of hydrogen production from an aqueous media including electron donors (Park and Kang 2007; Yuan et al. 2009). Metal oxides based on Nb like Nb_2O_5 with band gap = 3.4 eV can improved photocatalytic hydrogen evolution through coupling of Pt (Chen et al. 2007). The photoactivated splitting efficiency of water by the metal oxides of Ga_2O_3 with band gap = 4.6 eV and CeO_2 with d^{10} electronic configuration of metal ions is highly enhanced when coupled with Zn, Sr, Cr, Ta, Ba, Ca, and RuO_2 (Yanagida et al. 2004; Kadowaki et al. 2007).

Ternary Metal Oxides

Ternary metal oxide based on Ti with interlayered additives of TiO_2 shows efficient splitting reaction of water under UV light. The titanates with layered structures such as $K_2Ti_4O_9$, $Na_2Ti_3O_7$, and $K_2Ti_2O_5$ have enough photoactivity to hydrogen production via splitting reaction of water (Shibata et al. 1987). $LaTiO_3$ incorporated with NO- and Ba-doped in the presence of additive of alkaline hydroxide show permanent increasing of photocatalytic water splitting (Kim et al. 2005a). $SrTiO_3$

photocatalytic ability may be improved by some suitable metal cation coupling, such as La and Ga (Qin et al. 2007). Also, perovskite crystallite structure of $CaTiO_3$ with band gap = 3.5 doped with Zr shows higher photocatalytic performance under UV light (Sun et al. 2007). $K_4Nb_6O_{17}$ with layered structure show excellent photosplitting of water in an aqueous methanolic solution. The structure modified with cocatalysts of NiO, Au, Pt, and Cs perform increased photocatalytic activity for H_2 production (Sayama et al. 1998). Tantalate metal oxides like $LiTaO_3$ with band gap = 4.7 eV, $KTaO_3$ with band gap = 3.6 eV, and perovskite $NaTaO_3$ with band gap = 4.0 eV have high water splitting yields that mainly depend on band angles of Ta–O–Ta. Opening the angles near to 180° caused more easily transportation of electron–hole pairs and much reduction of the band gap. Some of W- and Mo-based heterogeneous materials show photoactive performance of water splitting just under UV light such as $PbWO_4$ with band gap = 3.9 eV and $PbMoO_4$ with band gap = 3.31 eV (Akihiko et al. 1990).

Visible Light-Activated Catalysts

The pure metal oxide usually bears some disadvantages of great resistivity and fast recombination pace of photo-produced charges. For example, WO_3, Bi_2WO_6, Bi_2MoO_6, and α-Fe_2O_3 have band gaps 2.8, 2.8, 2.7, and 2.2 eV, respectively, because positions of low conduction band do not have photoactivity about H_2 evolution (Aroutiounian et al. 2002; Ingler et al. 2004; Satsangi et al. 2008). Therefore, recent investigations try to improve the photoconductivity and low recombination rate of charges. One route is metal or non-metal doping to engineer the band gap energy. The electron donor species with higher levels of band gap than valence band of original photocatalyst, or electron acceptor ones with lower levels of band gap than original conduction band, provide wide ranges of band gap of metal oxides with visible light photoactivity. Coupling of TiO_2 with Pt^{4+} and Ag^+ increases the photocatalytic performance underneath both visible and UV irradiations (Kim et al. 2005b; Rengaraj and Li 2006). Pt^{4+} and Ag^+ metal ions participating in visible light absorption resulted in reducing of recombination rate. Using dye for sensitizing of metal oxides caused in reduction of wide band gap is another approaching method within improving the visible light sensitivity of water splitting. The process progresses with shift of excited electron of HOMO to LUMO of dye molecule and next transferring to conduction band of original photocatalysts. TiO_2 loaded with dye and $K_4Nb_6O_{17}$ show enhanced capability of H_2 evolution. Moreover, numerous coordination compounds Co(II), Zn(II), Pt(II), and Cr(II) with polypyridine, phthalocyanine, alizarine, and metalloporphyrins perform photocatalytic efficiency within H_2 generation (Shimidzu et al. 1985). A new heptazine-based porous organic polymer named POP–HE show intense visible light catalytic activity of oxidative conversion of benzyl alcohol to benzaldehyde. The researchers claimed that POP–HE compound has higher photocatalytic efficiency than graphite carbon nitride (Xu et al. 2019a). Another new research shows that anchoring of Pd nanoparticles to TiO_2 can permanently improve the

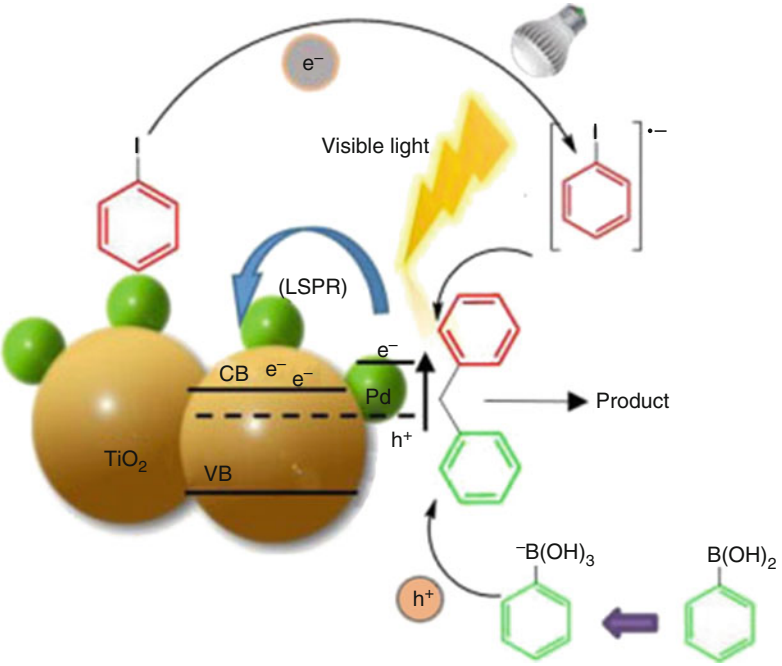

Fig. 9.9 Proposed mechanism of charge separation in Pd/TiO_2 compounds led to enhancement of Suzuki–Miyaura coupling reaction. LSPR represents localized surface plasmon resonance. (Reprinted with permission of Elsevier from Koohgard and Hosseini-Sarvari 2018)

photocatalytic activity of TiO_2 heterogeneous coupled catalyst within Suzuki–Miyaura coupling reaction. The applied synthetic method was resulted in reducing of recombination rate of hole–electron through the shown mechanism in Fig. 9.9 (Koohgard and Hosseini-Sarvari 2018). Li et al. introduced an effective coupled photocatalyst of $BiVO_4/Ag_2O$ with low band gap prepared with impregnation–evaporation technique. $BiVO_4/Ag_2O$ has shown higher photodegradation rate within methyl orange in comparison with pure $BiVO_4$ as a p–n heterojunction type (Li et al. 2015a). Also another p–n heterojunction semiconductor with $BiVO_4$ coupled with Cu_2O showed more photocatalytic degradation of methylene blue and colorless organic pollutant of phenol than $BiVO_4$ (Wang et al. 2013). The discussed and some more of visible light photocatalysts have been listed in Table 9.2.

9.3.2 Z-Scheme

Despite that many pure or couple metal oxides show suitable photocatalytic performance especially water splitting under irradiation of UV or visible light, some weaknesses diminish the quality of process:

Table 9.2 Photocatalysts coupled heterogeneously and the related usage

No.	Photocatalyst	Usage	References
1.	$TiO_2/Pt/RuO_2$	Water splitting/Rhodamine B	Duonghong et al. (1981)
2.	TiO_2/Ag_xO	Hydrogen evolution	Park and Kang (2007)
3.	Nb_2O_5/Pt	Hydrogen production	Chen et al. (2007)
4.	POP-HE	Benzyl alcohol oxidation	Xu et al. (2019a)
5.	TiO_2/Pd	Suzuki-Miyaura coupling	Koohgard and Hosseini-Sarvari (2018)
6.	BiVO4/Ag2O	Methyl Orange	Li et al. (2015a)
7.	$g\text{-}C_3N_4/BiOCl_xBr_{1-x}$	Rhodamine B and Rhodamine 640	Shi et al. (2014)
8.	Bi_5O_7I/Bi_2O_3	Malachite Green	Cheng and Kang (2015)

(a) A low percentage of light absorption up to the photocatalysts band gap
(b) Returned reaction of water formation

Beyond three interface kinds of heterojunction semiconductors, only type II bears acceptable photocatalytic activity. The conversion of type II with a direct Z-scheme mechanism can more increase the efficiency and suggests the solution for the abovementioned disadvantages. The system includes two photocatalysts coupled through redox charges carrying. The mentioned system is a biomimetic mechanism occurred in the photosynthesis reactions for transferring of the photo-induced electron of H_2O to nicotinamide adenine dinucleotide phosphate. The formed couple of heterojunction includes several photocatalysts species as the relevant redox potentials of the generated charges are held at higher capacity. Therefore, a recombination reaction of a small amount of electron−hole pairs causes them to be sacrifice that makes the excited charges with higher energies leave behind (see Fig. 9.10). The interesting mechanism provides the capability for visible photons with relatively low energies to promote an efficient degradation process. Since Z-scheme mechanism donates the mentioned benefits to a single photocatalyst having wide band gap, the respected studies have been greatly increased. Some of them are summarized in Table 9.3. One of notable study reports Pt-loaded in ZrO_2–TaON and Pt-loaded in WO_3 that demonstrate permanent photocatalytic H_2 generation from water with high apparent quantum yield at 420 nm. ZrO_2 extends the lifetime of the photogenerated charges and inhibition of the recombination because of modification of TaON n-type semiconductor (Maeda et al. 2010). A modified silver chromate with graphene oxide as binary Ag_2CrO_4–GO photocatalyst has shown notable degradation of methylene blue and phenol under visible light (Xu et al. 2015). The energy levels of conduction band and valence band for single Ag_2CrO_4 and graphene oxide were measured ca. 0.47 V and 2.27 V vs. NHE and ca. –0.75 V and 1.75 V vs. NHE, respectively. The photogenerated electrons of the conduction band of silver chromate combine with cavities of valence band from graphene oxide resulted in leaving of conduction band electrons of graphene oxide with higher potential and more negatively potential than the −0.28 V as potential value of O_2^{*-}/O_2. In some recent studies, the effective *Z*-scheme heterojunctions

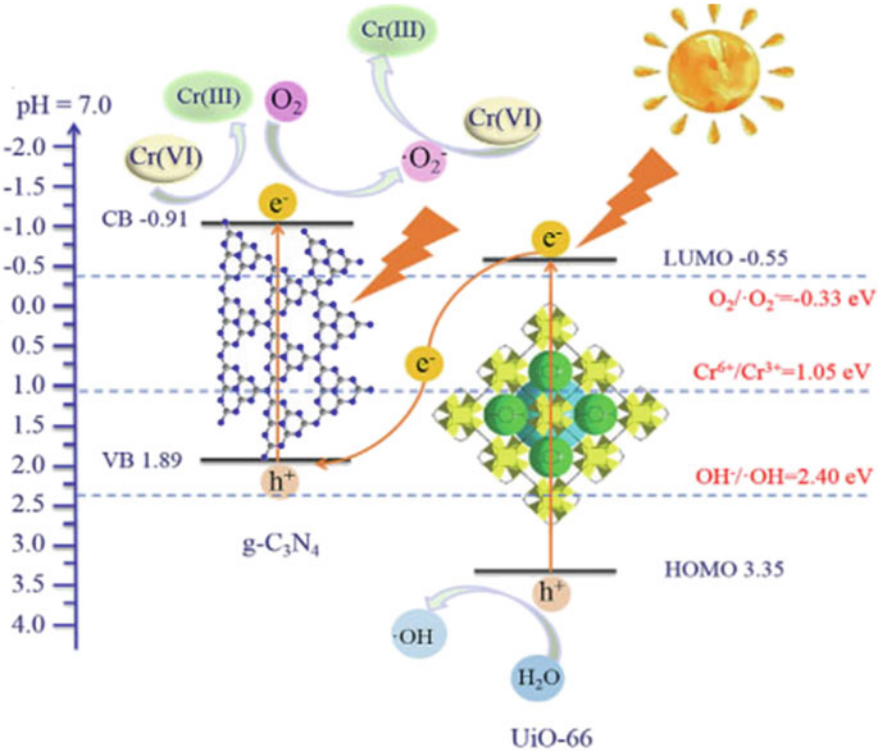

Fig. 9.10 A mechanistic view of photocatalytic Cr(VI) reduction mechanism of g-C_3N_4/UiO-66. HOMO energy of UiO-66 which is smaller than OH^-/$^*OH$ pairs caused to form $^*OH$ with oxidation of OH^- or H_2O. CB and VB stand for conductive band and valence band, respectively. (Reprinted with permission of Elsevier from Yi et al. 2019)

within visible light photocatalytic performance have been prepared by loading of cuprous oxide, graphite carbon nitride, bismuth oxide, cadmium sulfite, and metal organic frameworks (Li et al. 2019a; Yi et al. 2019; Hu et al. 2020; Wang et al. 2020; Xu et al. 2020). A new interesting one is a heterojunction of g-C_3N_4/UiO-66 (BG_xU_y) prepared by 3D UiO-66 and 2D g-C_3N_4 sheets through ball milling method. The superior improvement of Cr(VI) reduction upon white light irradiation was shown in comparison with both of single contents. Yi et al. (Yi et al. 2019) reported a facile fabrication of 2D/3D Z-scheme g-C_3N_4/UiO-66 heterojunction with enhanced photocatalytic Cr(VI) reduction performance under white light (see Fig. 9.10).

Table 9.3 Photocatalysts of *Z*-scheme modified and their summarized reaction

Sr. No.	Photocatalyst	Usage	References
1.	Pt-loaded WO_3 & Pt-loaded ZrO_2/TaON	Water splitting	Maeda et al. (2010)
2.	Ag_2CrO_4-GO	Methylene Blue and Phenol	Xu et al. (2015)
3.	Cu_2O/Bi_2MoO_6	Decontamination of Sulfadiazine and Ni(II)	Xu et al. (2020)
4.	CdS/polyimide (PI)	Hydrogen evolution	Hu et al. (2020)
5.	α-Fe_2O_3/d-C_3N_4 and α-Fe_2O_3/g-C_3N_4	Tetracycline	Wang et al. (2020)
6.	$BiOBr/Bi_{12}O_{17}Br_2$	Resorcinol degradation and NO removal	Li et al. (2019a)
7.	Tungsten trioxide/polyimide (PWO/PI)	Imidacloprid	Meng et al. (2018)
8.	Er3þ:$Y_3Al_5O_{12}$@$NiGa_2O_4$-MWCNTs-WO_3	Methylene Blue and Hydrogen evolution	Tang et al. (2019)

9.3.3 p−n Junction Materials

Other improved photocatalysts as dual semiconductors reported in literature are heterojunctions of two p-type and n-type semiconductors. The considered photocatalysts including trivalent and pentavalent additives, respectively, resulted in electron–hole generation in the electronic states of semiconductor (Beydoun et al. 2000; Spasiano et al. 2013). The designed p–n junctions of photocatalysts allow the charge transfer between two semiconductor contents through the direct contact. The structure provides the advantage of separation of charge carriers along with reduction of electron−hole pair recombination. The charge transfer mechanism in a general p–n junction type is illustrated in Fig. 9.11. Through the connection of two types of p–n semiconductors, a small content of electron from n-type is transferred to p-type. Therefore, the resulted hole in interfacial establishes an inner electric field where the n-type extends the positive charge and vice versa for p-type. The formed inner electric field prohibits to flux of the remaining hole and electron into the related negative and positive fields. Therefore, the effective charge separation and reduced recombination rate can be achieved.

The position of valence band of g-C_3N_4 as 1.89 eV vs. NHE is more in comparison with $OH^-/{}^*OH$ standard potential with 2.40 eV vs. NHE, so photo-excited holes on g-C_3N_4 will not respond with OH^-/H_2O to form ${}^*OH$. It can be rephrased that HOMO energy of UiO-66 with 3.35 eV vs. NHE is smaller than $OH^-/{}^*OH$ pairs with 2.40 eV vs. NHE, caused to form ${}^*OH$ with oxidation of OH^- or H_2O.

Lee et al. (Kim et al. 2017; Chae et al. 2019) introduced some p–n junction having photocatalytic behavior or usable in diodes/solar cells with semiconductor combination, viz., p-poly(3-hexylthiophene)/n-ZnO and p-Co_3O_4/n-ZnO. For the first one

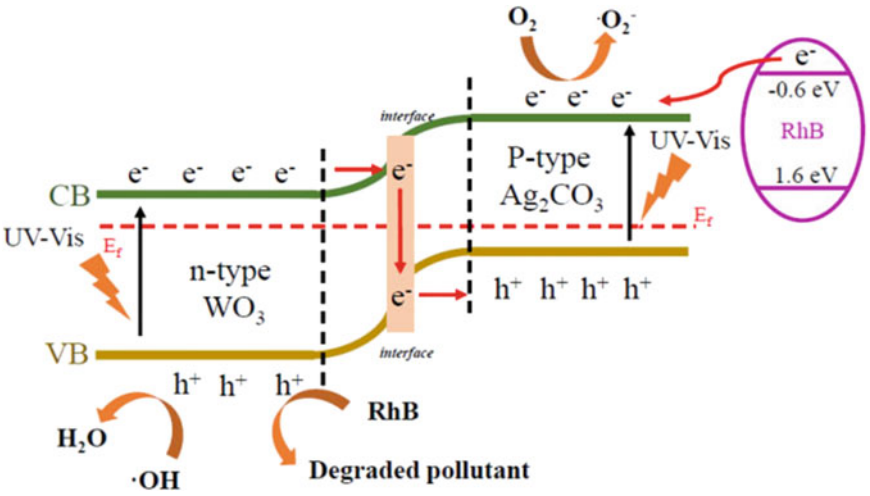

Fig. 9.11 Photoexcited electron–hole separation in n–p heterojunction WO_3-Ag_2CO_3 at photocatalytic degradation process of Rhodamine B. CB and VB stand for conductive band and valence band, respectively. RhB stands for Rhodamine B. (Reprinted with permission of Elsevier from Gao et al. 2019)

Table 9.4 *p-n* heterojunction photocatalysts and the summarized usage

Number	Photocatalyst	Usage	References
1.	TiO_2/Cu(II)	Production of Benzaldehyde	Spasiano et al. (2013)
2.	TiO_2/Fe_3O_4	Photodissolution	Beydoun et al. (2000)
3.	p-WO_3/n-Ag_2CO_3	Rhodamine B	Gao et al. (2019)
4.	p-P3HT/n-ZnO	Rhodamine 6G	Chae et al. (2019)
5.	p-Co_3O_4/n-ZnO	Light-Emitting Diode	Kim et al. (2017)

through self-grown organic content over ZnO surface, the hybrid p–n junction was prepared. It shows the catalysis activity for Rhodamine 6G degradation (Chae et al. 2019) and the next one prepared from aqueous media at low temperature and growing of ZnO over Co_3O_4 having light-emitting diode property (Kim et al. 2017). Some of more recent introduced p–n heterojunction photocatalyst are collected in Table 9.4.

9.3.4 Ion-Exchangeable Semiconductors

The wide range of ion-exchangeable compounds with layered structures can be classified into oxides and hydroxides. The ion-exchangeable compounds bear zigzag lepidocrocite sheet type intercalated with counter ions of hydrates protons arrive with high capability of solar energy utilization. As above discussed, adequate

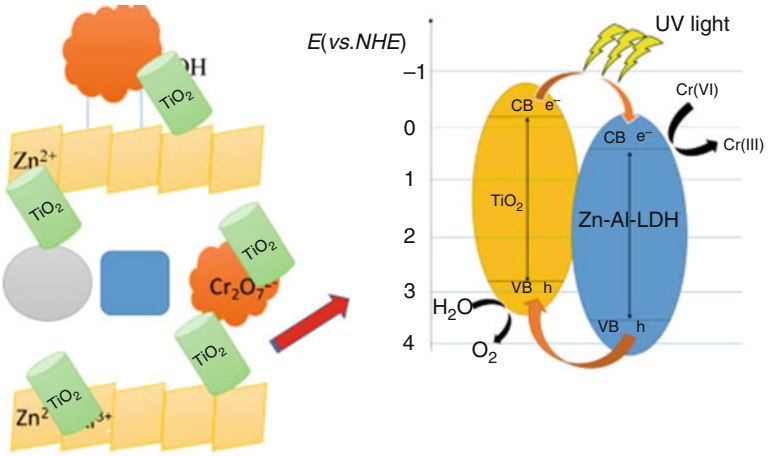

Fig. 9.12 Photocatalytic reduction of Cr(VI) using Zn-Al-layered double hydroxide and TiO2 composites. CB and VB stand for conductive band and valence band, respectively. (Reprinted with permission of Elsevier from Yang et al. 2019)

separation of electron–hole with low recombination rate is a key involving factor of performance of photo-remediation, water splitting, and general photocatalytic applications. An advanced method to gain the purpose of adequate separation of electron–hole is structural manipulation of layered materials with interstitial inserting of heteroatoms to engineering charge transfer procedure (Zong et al. 2011; Gao et al. 2013; Xiong et al. 2016; Cui et al. 2017; Li et al. 2017a; Cao et al. 2018). Further alternative structure is two-dimensional layered double hydroxide having general formula of $[M_{1-x}^{2+}M_x^{3+}(OH)_2]^{x+}(A^{n-1})_{x/n}.mH_2O$. The negatively charged A anion is accommodated betwixt of positive-charged M layers of two various divalent and trivalent metal ions (Chen et al. 2019; Jo et al. 2019; Li et al. 2019b; Wang et al. 2019a; Yang et al. 2019). Generally, the main applicable researching fields on ion-exchangeable materials can be highlighted as dye degradation, removal of toxic gaseous like NO, toluene, and so on, water splitting, light-emitting diode, solar cell, Cr(VI) reduction, CO_2 transformation to carbonic fuel like methane, and so on (Zong et al. 2011; Gao et al. 2013; Xiong et al. 2016; Cui et al. 2017; Lee et al. 2017; Li et al. 2017a, 2018c, 2019b; Cao et al. 2018; Chen et al. 2019; Yang et al. 2019; Jo et al. 2019; Wang et al. 2019a). The reported ion-exchangeable layered sheets having negatively charged particles intercalated between layers with positive charge have different species like carbonate/Zn, ZnNi and ZnCu hydroxides, carbonated/Bi_2WO_6, TiO_2/polyvinyl alcohol, alkaline metal ions/carbon nitride, NO_3^-/g-C_3N_4, and so on. As obviously illustrated in Fig. 9.12, the titania nanoparticles were uniformly intercalated in the layered double hydroxide of Zn–Al. The combination of TiO_2/Zn–Al–layered double hydroxide is the main reason for enhancing performance of transformation of photogenerated electron–hole and separation for reduction of Cr(VI) (Yang et al. 2019).

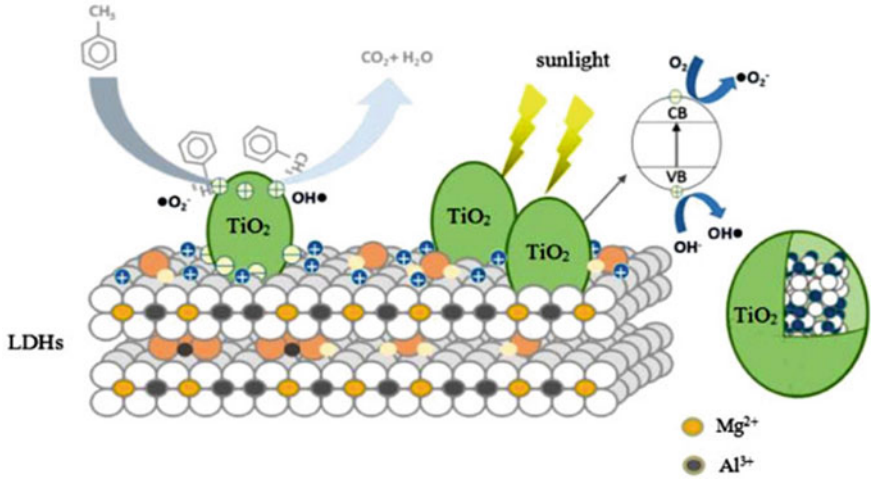

Fig. 9.13 A proposed photocatalytic mechanism of TiO_2@ layered double hydroxide under simulated sunlight. CB and VB stand for conductive band and valence band, respectively. LDH represent layered double hydroxide. (Reprinted with permission of Elsevier from Wang et al. 2019a)

Lee et al. (Lee et al. 2017) claimed to fabrication of sandwich structures bear transparent pliable light-emitting diodes with capable usage in wearable electronic instruments with transparent textiles. Lee et al. (Lee et al. 2017) used electrospinning method to intercalating light-emitting diodes of ZnO@graphene quantum dots in transparent nanofiber textile to safeguard QLED devices versus the degradation. Lee et al. (Lee et al. 2017) attended the obtained results can inspire new-generation methods of wearable electronic cloths and so on.

Moreover, Wang et al. (2019a) reported a new synthesized TiO_2@ layered double hydroxide having permanent photocatalytic degradation of gaseous toluene under true sunlight irradiation. Actually, TiO_2 was formed through hydrolyzation of tetrabutyl titanate over initially designed MgAl-layered double hydroxide substrate. Large surface area of designed substrate, acceptable separation of generated hole and electron charges, and existence of necessity amount of $OH^{\bullet}$ and $^{\bullet}O_2^-$ radicals are the main reasons of highly observed photocatalytic efficiency. For more information see proposed mechanism in Fig. 9.13.

Along with photodegradation of organic pollutants like dyes, the ion-exchangeable intercalated and layered double hydroxides show the ability for hydrogen and oxygen generation and energy production. Some of the interested recently reported results have been listed in Table 9.5.

Table 9.5 Ion-exchangeable photocatalysts having layered structure and their summarized applications

Number	Photocatalyst	Application	References
1.	Li/g-C_3N_4	Rhodamine B	Zhang et al. (2019)
2.	PbS-CdS/Ti_6O_{13}	Reactive Black 5	Sehati and Entezari (2017)
3.	g-C_3N_4 NT/rGO	Rhodamine B	Wei et al. (2019)
4.	RGO@ZnAlTi-LDO	Cr(VI) reduction	Ye et al. (2019)
5.	Nd/CoAL LDH	Acid Red 14/Ciprofloxacin/ Ibuprofen	Khodam et al. (2018)
6.	$CoNiSe_2$ LDH	Hydrogen evolution	Yang et al. (2019b)
7.	NiFeSP/Nickel Foam	Hydrogen evolution	Xue and Sun (2019)
8.	CoO*x*/ZnS@CdS/ Ni	Hydrogen production	Xin et al. (2018)

9.3.5 Photocatalytic Compounds Kind

Numerous photocatalysts have prepared and examined the activity toward environmental purification. Many of them show high performance under UV irradiation. Finally, there have been continual tries to development and improvement of visible light photocatalytic efficiency. The related efforts necessitate more studies of physicochemical properties of powerful photocatalysts.

TiO_2 as one of known powerful photocatalyst can be modified to achieve higher than promising results of photocatalytic activity. The sophistication include loading of TiO_2 with carbon, fullerene, graphite, activated carbon, different forms of grapheme oxide, nanosheets, single-walled carbon nanotubes, multiple-walled carbon nanotube, and so on (Wu et al. 2010; Cong et al. 2011; Meng and Oh 2012; Mohammadi and Sabbaghi 2014; Rong et al. 2015). However, some alternative modifications have been attended on the incorporation of metallic and nonmetallic elements (such as S, I, N, La, and Fe) in related structure (Li et al. 2011; Collazzo et al. 2012; Niu et al. 2013). Loaded TiO_2 over MWCNT using a modified sol−gel technique was shown better activity of TiO_2/MCNT composite within photodegradation of Reactive Black 5 dye in comparison with function of single TiO_2 (Hamid et al. 2014). Except modifications of titania, the photocatalysts can be widely classified as oxides, oxyhalides, and sulfides of metals and non-metals. In addition, their combinations and composite compounds have been investigated on different substrates. Actually, the catalytic performances of modified titania compounds for contaminant photodegradation for irradiation of UV-visible-solar light were examined. Table 9.6 was subdivided with numerous recent reported photocatalysts having high efficient performance.

Table 9.6 Routine classification of effective visible/solar light photocatalysts

Number	Class	Photocatalyst	Irradiation	Dye/pollutant	Light time	Destruction	References
1.	Bi_2S_3	Bi_2S_3 coated on Stainless steel mesh	Natural sunlight	Cr (VI)/Rhodamine B	60 min	Photodegradation of single mode of 10 ppm Cr(VI) and binary mixture of 10 ppm Cr(VI) and 5 ppm RhB	Chahkandi and Zargazi (2019)
2.	$BiFeO_3$	Coated on SS mesh	Natural sunlight	Phenol	30 min		Zargazi and Entezari (2019a)
3.	Bi_2WO_6	Coated on SS mesh	Natural sunlight	4Nitrophenol/chlorophenol	140 min		Zargazi and Entezari (2019b)
4.	Bi_2WO_6	Flower like powder	Natural sunlight	Rhodamine B/Methylene Blue	30 min		Zargazi and Entezari (2018)
5.	g-C_3N_4	Heptazine-based g-C_3N_4	Natural sunlight	Water splitting	–	High efficient visible light photocatalyst of C_6N_7 monolayer for water splitting	Liu et al. (2019)
6.	BiOC	Ag@Ag_2O/BiOC	150 W xenon	Rhodamine B	120 min	Heterojunction of Ag@Ag2O/BiOC as efficient photodegradation of 10 ppm RhB	Zhao et al. (2019)
7.	BiOBr	p-n junction of Bi4Ti3O12/BiOBr	$\lambda > 400$ nm	Ciprofloxacin/tetracycline	180 min	p-n junction of Bi4Ti3O12/BiOBr as photodegradation of 20 ppm CIP/TC	Shen et al. (2019)
8.	$BaTa_2O_6$:Ir,La/$SrTiO_3$:Ir	Z-scheme $BaTa_2O_6$ and $SrTiO_3$doped with Ir and La	300 W Xe lamp	Water splitting	–	Z-scheme $BaTa_2O_6$:Ir,La/$SrTiO_3$:Ir as effective for H_2 and O_2 evolution	Kudo et al. (2019)

(continued)

Table 9.6 (continued)

Number	Class	Photocatalyst	Irradiation	Dye/pollutant	Light time	Destruction	References
9.	Fluorescein	Fluorescein	10 W blue LED lamp	Synthesis of benzimidazoles		Benzimidazoles synthesis from aromatic aldehydes and o-phenylenediamines	Li et al. (2019f)
10.	FeOCPc	FeOCPc@Ni	Sunlight lamp (220 V, 8 W, white light LED)	Methyl orange and p-nitrophenol	30 min	Degradation of 97.91% and 97.99% of MO and PNP by (FeOCPc@Ni)	Ma et al. (2019)
11.	RGO	Silver doped RGO	350–370 nm	Oxidative coupling of benzylamines	12 h	Plasmonic photocatalyst of silver for benzylamines coupling	Kumar et al. (2019)
12.	Amine functionalised ZnCr LDH–MCM-41	Au/Pd alloy on an amine functionalised ZnCr LDH–MCM-41	300 wt xenon lamp	One-pot imine synthesis	45 min	Au/Pd bimetallic alloy loaded amine (APTES) functionalised LDH (Layered double hydroxide)–MCM-41 composite for imine synthesis	Sahoo et al. (2019)
13.	MOF	Pt/[Zn2(BODIPY)(BPDC)2]·H2O	420 nm	Hydrogen production	–	Visible photocatalyst of pillared-paddlewheel type metal-organic frameworkdecorated with Pt nanoparticles for efficient H2 generation	Yang et al. (2019a)
14.	BVO_4	Z-scheme ZnRh2O4/Au/BiVO4	Xenon lamp $\lambda > 400$ nm	Liberation of H_2 and O_2	–	Hierarchical structure of efficient photocatalyst of $ZnRh_2O_4$/Au/$BiVO_4$ for production of H_2 and O_2	Takashima et al. (2019)

9.4 Future Remarks and Limitations

During the twentieth century and for future enhancing outlook, one of the main universal fears should be environmental remediation aspects. The required energy for remediation and environmental have close dependence about numerous issues having interplaying effects. The ultimate goal of green remediation for minimizing the greenhouse gas emissions needs most spending efforts. The well-known different nanomaterials have been introduced to achieve detection and elimination of pathogens. The respected nanomaterials can act through applicable routes with high sensitivity, lower cost, in-line and real-time detection, lower turnaround times, and more throughput and transportability in environmental purification. Among them, nanomaterials of metal oxide and metal especially chemical-functionalized ones can be utilized for removal of aqueous and aerial organic pollutants. Further improvements have to be exerted in selective and complete photocatalytic remediation through degradation of contaminants to non-toxic products to changing of pH and concentration of chemical staffs and cost optimization. TiO_2 has been considered one of the most effective ones because of its stability and some other advantages. However, several efforts have been and are being followed to decrease the major failure of TiO_2 to enhance usage in a huge area of solar light for more asked applications. The original importance of sophistication of proper band gap and chemistry of surface/interface addressed the required researches. The appropriate studies are (i) usage of metals–non-metals having general suitable characters as semiconductor, surface plasmon resonance, and so on, (ii) introduction of novel composite compounds; (iii) study of the effect of dopants–additives–sensitizers; (iv) finding the catalytic mechanism; (v) production of thin films of photocatalysts within titania, alumina, stainless steel, and molecular sieves; (vi) enhancing the effective surface area of photocatalyst; (vii) development of more sensitive photocatalyst in natural sunlight against of fictional light; and (viii) applying of diverse synthesis methods such as hydrothermal, co-precipitation, electrochemical, sol–gel, and so on. Another important challenge regarded to designing of appropriate photoreactor and the commercial concerns. Despite the great contents of mercantile contaminants needing remedy, the running conditions of technology should not be enough. However, at first an effective multiphasic impact of pollutant, oxygen, solar light, and photocatalyst is required. In order to commercialize of scale implementation for reliable scale-up, the specification of eminent factors and simulation of a reliable rate declaration are necessary. Investigations are still pursuing to improve quantum yield and maximize the impact of substances and photons regarding fluctuations in solar irradiation. Nonetheless, designing of photoreactors are followed according to alternative and approximate kinetic statements. Main designs of a photoreactor are performed for concentrating collector–reactor, compound parabolic collector–reactor, and non-concentrating collector one (Blanco et al. 2009; Braham and Harris 2009; Spasiano et al. 2015). Of the related more routine designs, compound parabolic collector–reactor includes more advantages about utilizing both of beam and reactive components and is resulted as the most modern

and applicable design (Tanveer and Tezcanli Guyer 2013). However, even the perfected design involved with some process limitations include (i) more effective performance for oxidative process like dyes with low concentration, (ii) sensitivity to mutability in solar intensity, (iii) complete contact of catalyst and effluent and then asking for separation of catalyst and treated effluent, and (iv) far from of headed commercialization. Resolving the last case along with commercial livability needs a facile, cost-effective, sustainable, and safety operation. To achieve the respected goals and minimize the pertinent limitations, it seems employing of proper UV-visible light photocatalysts is promised.

9.5 Conclusions

One can state that the best technique and material for pesticide removing can be chosen according to all involved parameters such as pH, temperature, quantity of contaminated environments, kind of matrix, and solubility of pesticides. The applied physicochemical process of pesticides remediation is permanently based on the forms of usage energy to degradation of the related pollutants, along with photolysis, ultrasound, and the other alternative methods. For purpose of pesticides remediation, metal oxide photocatalysts like TiO_2 using Fenton reactions joined to light, electric current, and ultrasound can highly extend the destruction of pesticides especially in aqueous phase. However, the current study was furnishedthe fundamental issues of the photocatalytic process. The most important ones contents are appropriate mechanism, thermodynamics, kinetics and recombination of reaction, suggested mechanism of an active photocatalyst, and the impact of effective factors on photocatalytic performance. Typical heterogeneous photocatalysis progresses by generation of electron–hole pairs commenced through band gap agitation of particle of a semiconductor. Adsorption of a photon with required potential equal or greater than band gap as the initial necessity of photocatalytic reactions resulted in electron transition from valence band to conduction band. Desired thermodynamically catalytic process can be evaluated based on intrinsic, apparent, and official quantum yield and efficiency of conversion. Conclusive measurement of total carbon content of the contaminants in terms of TOC or COD can be used to quantity determination of the photoreaction rate in a pseudo-L–H model. Since visible light active photocatalysts have small band gap energy, arresting of charge recombination is needful. The main mechanisms of effectual excitation and charge pair separation have been noted and discussed with clear examples. The governed parameters influencing on photocatalytic activity have been studied at length, completed with accounted results in literature. The parameters are (i) intrinsic photocatalyst type related to contents and band structure, (ii) irradiation energy effect on the number of generated electron–hole pairs, (iii) kind and character of pollutants having different functional groups, (iv) scattering and blockage of adventure light that can restrict the amount of loaded catalyst into the system, (v) pH of media and substrate, and (vi) value and property of dopant in composited catalyst−substrate influenced on surface

chemistry. However, a plenary path across for achieving optimized factors should be figured out. For applicable scale-up of photocatalysis process, an impact face of the photocatalyst and contaminant/goal, irradiation light, and O_2 should be provided. Finally, the most attended conclusions can be derived from the presented review chapter as:

1. Effective photocatalysis using natural sunlight energy and without any new generated footprint can decolorized/degrade the industrial effluent including paints and/or organics.
2. Manipulation of a photocatalyst band gap by hetero-coupling with the purpose of extending of absorption of visible region of spectrum.
3. Investigation of effective parameters can be useful to improve the photocatalytic performance.

Acknowledgments MCH highly appreciates for the financial support by the Hakim Sabzevari University, Sabzevar, Iran.

References

Ahmed I, Iqbal HMN, Dhama K (2017) Enzyme-based biodegradation of hazardous pollutants – an overview. JEBAS 5(4):402–411

Akihiko K, Kazunari D, Ken-ichi M, Onishi T (1987) Photocatalytic activities of TiO_2 loaded with NiO. Chem Phys Lett 133:517–519

Akihiko K, Steinberg M, Bard AJ et al (1990) Photoactivity of ternary lead-group IVB oxides for hydrogen and oxygen evolution. Catal Lett 5:61–66

Andreozzi R, Caprio V, Ermellino I et al (1996) Ozone solubility in phosphate-buffered aqueous solutions: effect of temperature, tert-butyl alcohol, and pH. Ind Eng Chem Res 35:1467–1471

Andreozzi R, Caprio V, Insola A, Marotta R (1999) Advanced oxidation processes (AOP) for water purification and recovery. Catal Today 53:51–59. https://doi.org/10.1016/S0920-5861(99)00102-9

Aroutiounian VM, Arakelyan VM, Shahnazaryan GE et al (2002) Investigation of ceramic Fe_2O_3 ⟨Ta⟩ photoelectrodes for solar energy photoelectrochemical converters. Int J Hydrog Energy 27:33–38. https://doi.org/10.1016/S0360-3199(01)00085-4

Asmatulu R (2015) Photo-active metal oxide nanomaterials for water splitting. Sci Lett J 169

Asmatulu R, Haynes H, Shinde M et al (2010) Magnetic characterizations of sol-gel-produced Mn-doped ZnO. J Nanomater 2010:80–83. https://doi.org/10.1155/2010/715282

Asmatulu R, Ceylan M, Nuraje N (2011) Study of superhydrophobic electrospun nanocomposite fibers for energy systems. Langmuir 27:504–507. https://doi.org/10.1021/la103661c

Babuponnusami A, Muthukumar K (2014) A review on Fenton and improvements to the Fenton process for wastewater treatment. J Environ Chem Eng 2:557–572. https://doi.org/10.1016/j.jece.2013.10.011

Bai X, Wang L, Zong R, Zhu Y (2013) Photocatalytic activity enhanced via g-C_3N_4 nanoplates to nanorods. J Phys Chem C 117:9952–9961. https://doi.org/10.1021/jp402062d

Barrera-Salgado KE, Ramírez-Robledo G, Álvarez-Gallegos A, Pineda-Arellano CA, Sierra-Espinosa FZ, Hernández-Pérez JA, Silva-Martínez S (2016) Fenton process coupled to ultrasound and UV light irradiation for the oxidation of a model pollutant. J Chem 2016:1–7

Beard MC, Luther JM, Nozik AJ (2014) The promise and challenge of nanostructured solar cells. Nat Nanotechnol 9:951–954. https://doi.org/10.1038/nnano.2014.292

Bellardita M, García-López EI, Marcì G et al (2018) Selective photocatalytic oxidation of aromatic alcohols in water by using P-doped g-C_3N_4. Appl Catal B Environ 220:222–233. https://doi.org/10.1016/j.apcatb.2017.08.033

Beydoun D, Amal R, Low GKC, McEvoy S (2000) Novel photocatalyst: titania-coated magnetite. Activity and photodissolution. J Phys Chem B 104:4387–4396

Blanco J, Malato S, Fernández-Ibañez P et al (2009) Review of feasible solar energy applications to water processes. Renew Sust Energ Rev 13:1437–1445. https://doi.org/10.1016/j.rser.2008.08.016

Bokare AD, Choi W (2014) Review of iron-free Fenton-like systems for activating H2O2 in advanced oxidation processes. J Hazard Mater 275:121–135

Braham RJ, Harris AT (2009) Review of major design and scale-up considerations for solar photocatalytic reactors. Ind Eng Chem Res 48:8890–8905. https://doi.org/10.1021/ie900859z

Cai J, Wu X, Li S, Zheng F (2017) Controllable location of Au nanoparticles as cocatalyst onto TiO_2@CeO_2 nanocomposite hollow spheres for enhancing photocatalytic activity. Appl Catal B Environ 201:12–21. https://doi.org/10.1016/j.apcatb.2016.08.003

Cao S, Li H, Tong T et al (2018) Single-atom engineering of directional charge transfer channels and active sites for photocatalytic hydrogen evolution. Adv Funct Mater 1802169:1–9. https://doi.org/10.1002/adfm.201802169

Chae S, Yu J, Oh JY, Lee T (2019) Hybrid poly (3-hexylthiophene) (P_3HT) nanomesh/ZnO nanorod p-n junction visible photocatalyst for efficient indoor air purification. Appl Surf Sci 496:143641. https://doi.org/10.1016/j.apsusc.2019.143641

Chahkandi M, Zargazi M (2019) Novel method of square wave voltammetry for deposition of Bi2S3 thin film: photocatalytic reduction of hexavalent Cr in single and binary mixtures. J Hazard Mater 380:120879

Cheng L, Kang Y (2015) Bi5O7I/Bi2O3 composite photocatalyst with enhanced visible light photocatalytic activity. Catal Commun 72:16–19

Che W, Cheng W, Yao T et al (2017) Fast photoelectron transfer in (Cring)-C_3N_4 plane heterostructural nanosheets for overall water splitting. J Am Chem Soc 139:3021–3026. https://doi.org/10.1021/jacs.6b11878

Chen X, Yu T, Fan X et al (2007) Enhanced activity of mesoporous Nb_2O_5 for photocatalytic hydrogen production. Appl Surf Sci 253:8500–8506. https://doi.org/10.1016/j.apsusc.2007.04.035

Chen L, He J, Liu Y, Chen P, Au C-T, Yin S-F (2016) Recent advances in bismuth-containing photocatalysts with heterojunctions. Chin J Catal 37(6):780–791

Chen C, Zeng H, Yi M et al (2019) In-situ growth of Ag_3PO_4 on calcined Zn-Al layered double hydroxides for enhanced photocatalytic degradation of tetracycline under simulated solar light irradiation and toxicity assessment. Appl Catal B Environ:47–54. https://doi.org/10.1016/j.apcatb.2019.03.083

Collazzo GC, Foletto EL, Jahn SL, Villetti MA (2012) Degradation of direct black 38 dye under visible light and sunlight irradiation by N-doped anatase TiO_2 as photocatalyst. J Environ Manag 98:107–111. https://doi.org/10.1016/j.jenvman.2011.12.029

Cong Y, Li X, Qin Y et al (2011) Carbon-doped TiO_2 coating on multiwalled carbon nanotubes with higher visible light photocatalytic activity. Appl Catal B Environ 107:128–134. https://doi.org/10.1016/j.apcatb.2011.07.005

Cui W, Li J, Cen W et al (2017) Steering the interlayer energy barrier and charge flow via bioriented transportation channels in g-C_3N_4: enhanced photocatalysis and reaction mechanism. J Catal 352:351–360. https://doi.org/10.1016/j.jcat.2017.05.017

Da Rosa AV (2012) Fundamentals of renewable energy processes, 3rd edn. Academic, New York

Da Silva ES, Moura NMM, Coutinho A et al (2018) β–Cyclodextrin as a precursor to holey C–doped g–C_3N_4 nanosheets for photocatalytic hydrogen generation. ChemSusChem 11:2639–2639. https://doi.org/10.1002/cssc.201801789

Deng Y, Tang L, Feng C et al (2018) Construction of plasmonic Ag modified phosphorous-doped ultrathin g-C_3N_4 nanosheets/$BiVO_4$ photocatalyst with enhanced visible-near-infrared response

ability for ciprofloxacin degradation. J Hazard Mater 344:758–769. https://doi.org/10.1016/j.jhazmat.2017.11.027

Di T, Zhu B, Cheng B et al (2017) A direct Z-scheme g-C_3N_4/SnS_2 photocatalyst with superior visible-light CO_2 reduction performance. J Catal 352:532–541. https://doi.org/10.1016/j.jcat.2017.06.006

Dong B, Li M, Chen S et al (2017) Formation of g-C_3N_4@$Ni(OH)_2$ honeycomb nanostructure and asymmetric supercapacitor with high energy and power density. ACS Appl Mater Interfaces 9:17890–17896. https://doi.org/10.1021/acsami.7b02693

Duonghong D, Borgarello E, Grätzel M (1981) Dynamics of light–induced water cleavage in colloidal systems. J Am Chem Soc 103:4685–4690. https://doi.org/10.1021/ja00406a004

Feng R, Lei W, Sui X et al (2018) Anchoring black phosphorus quantum dots on molybdenum disulfide nanosheets: a 0D/2D nanohybrid with enhanced visible–and NIR −light photoactivity. Appl Catal B Environ 238:444–453. https://doi.org/10.1016/j.apcatb.2018.07.052

Frank AJ, Kopidakis N, Van De Lagemaat J (2004) Electrons in nanostructured TiO_2 solar cells: transport, recombination and photovoltaic properties. Coord Chem Rev 248:1165–1179. https://doi.org/10.1016/j.ccr.2004.03.015

Fu J, Yu J, Jiang C, Cheng B (2018) g-C_3N_4-based heterostructured photocatalysts. Adv Energy Mater 8:1–31. https://doi.org/10.1002/aenm.201701503

Fu J, Xu Q, Low J et al (2019) Ultrathin 2D/2D WO_3/g-C_3N_4 step-scheme H_2-production photocatalyst. Appl Catal B Environ:556–565. https://doi.org/10.1016/j.apcatb.2018.11.011

Fujishima A, Zhang X, Tryk DA (2008) TiO_2 photocatalysis and related surface phenomena. Surf Sci Rep 63:515–582. https://doi.org/10.1016/j.surfrep.2008.10.001

Gao H, Yan S, Wang J et al (2013) Towards efficient solar hydrogen production by intercalated carbon nitride photocatalyst. Phys Chem Chem Phys 15:18077–18084. https://doi.org/10.1039/c3cp53774a

Gao M, You L, Guo L, Li T (2019) Fabrication of a novel polyhedron-like WO_3/Ag_2CO_3 p-n junction photocatalyst with highly enhanced photocatalytic activity. J Photochem Photobiol A Chem 374:206–217. https://doi.org/10.1016/j.jphotochem.2019.01.022

Ghows N, Entezari MH (2013) Kinetic investigation on sono-degradation of reactive black 5 with core–shell nanocrystal. Ultrason Sonochem 20(1):386–394

Gogate PR, Pandit AB (2004a) A review of imperative technologies for wastewater treatment I: oxidation technologies at ambient conditions. Adv Environ Res 8:501–551. https://doi.org/10.1016/S1093-0191(03)00032-7

Gogate PR, Pandit AB (2004b) A review of imperative technologies for wastewater treatment II: hybrid methods. Adv Environ Res 8:553–597. https://doi.org/10.1016/S1093-0191(03)00031-5

Hamid SBA, Tan TL, Lai CW, Samsudin EM (2014) Multiwalled carbon nanotube/TiO_2 nanocomposite as a highly active photocatalyst for photodegradation of Reactive Black 5 dye. Chin J Catal 35:2014–2019. https://doi.org/10.1016/S1872-2067(14)60210-2

Hao X, Zhou J, Cui Z et al (2018) Zn-vacancy mediated electron-hole separation in ZnS/g-C_3N_4 heterojunction for efficient visible-light photocatalytic hydrogen production. Appl Catal B Environ 229:41–51. https://doi.org/10.1016/j.apcatb.2018.02.006

Herrmann JM (1995) Heterogeneous photocatalysis: an emerging discipline involving multiphase systems. Catal Today 24:157–164. https://doi.org/10.1016/0920-5861(95)00005-Z

Hoffmann MR, Martin ST, Choi W, Bahnemann DW (1995) Environmental applications of semiconductor photocatalysis. Chem Rev 95:69–96. https://doi.org/10.1021/cr00033a004

Homem V, Santos L (2011) Degradation and removal methods of antibiotics from aqueous matrices – a review. J Environ Manag 92(10):2304–2347

Hu Y, Hao X, Cui Z et al (2020) Enhanced photocarrier separation in conjugated polymer engineered CdS for direct Z–scheme photocatalytic hydrogen evolution. Appl Catal B Environ 260:118131. https://doi.org/10.1016/j.apcatb.2019.118131

Ingler WB, Baltrus JP, Khan SUM (2004) Photoresponse of p-type zinc-doped iron(III) oxide thin films. J Am Chem Soc 126:10238–10239. https://doi.org/10.1021/ja048461y

Jayaweera I (2003) Chemical degradation methods for wastes and pollutants, Environmental science and pollution control series. CRC Press, Boca Raton, pp 121–163

Jiang L, Yuan X, Zeng G et al (2018a) A facile band alignment of polymeric carbon nitride isotype heterojunctions for enhanced photocatalytic tetracycline degradation. Environ Sci Nano 5:2604–2617. https://doi.org/10.1039/C8EN00807H

Jiang L, Yuan X, Zeng G et al (2018b) Metal-free efficient photocatalyst for stable visible-light photocatalytic degradation of refractory pollutant. Appl Catal B Environ 221:715–725. https://doi.org/10.1016/j.apcatb.2017.09.059

Jin H, Bu Y, Li J et al (2018) Strong graphene 3D assemblies with high elastic recovery and hardness. Adv Mater 30:1–8. https://doi.org/10.1002/adma.201707424

Jo W-K, Kumar S, Tonda S (2019) N-doped C dot/CoAl-layered double hydroxide/g-C_3N_4 hybrid composites for efficient and selective solar-driven conversion of CO_2 into CH_4. Compos Part B Eng 176:107212. https://doi.org/10.1016/j.compositesb.2019.107212

Kadowaki H, Saito N, Nishiyama H, Inoue Y (2007) RuO_2-loaded Sr^{2+}-doped $CeO_2$with d^0 electronic configuration as a new photocatalyst for overall water splitting. Chem Lett 36:440–441. https://doi.org/10.1246/cl.2007.440

Kay A, Cesar I, Grätzel M (2006) New benchmark for water photooxidation by nanostructured α-Fe_2O_3 films. J Am Chem Soc 128:15714–15721. https://doi.org/10.1021/ja064380l

Khodam F, Amani-Ghadim HR, Aber S, Amani-Ghadim AR, Ahadzadeh I (2018) Neodymium doped mixed metal oxide derived from CoAl-layered double hydroxide: considerable enhancement in visible light photocatalytic activity. J Ind Eng Chem 68:311–324

Kim J, Hwang DW, Kim HG et al (2005a) Highly efficient overall water splitting through optimization of preparation and operation conditions of layered perovskite photocatalysts. Top Catal 35:295–303. https://doi.org/10.1007/s11244-005-3837-x

Kim S, Hwang S, Choi W (2005b) Visible light active platinum-ion-doped TiO_2 photocatalyst. J Phys Chem B 109:24260–24267

Kim JW, Lee SJ, Biswas P et al (2017) Solution-processed n-ZnO nanorod/p-Co_3O_4 nanoplate heterojunction light-emitting diode. Appl Surf Sci 406:192–198. https://doi.org/10.1016/j.apsusc.2017.02.129

Koohgard M, Hosseini-Sarvari M (2018) Enhancement of Suzuki–Miyaura coupling reaction by photocatalytic palladium nanoparticles anchored to TiO_2 under visible light irradiation. Catal Commun 111:10–15. https://doi.org/10.1016/j.catcom.2018.03.026

Kudo A, Yoshino S, Tsuchiya T, Udagawa Y, Takahashi Y, Yamaguchi M, Ogasawara I, Matsumoto H, Iwase A (2019) Z-scheme photocatalyst systems employing Rh- and Ir-doped metal oxide materials for water splitting under visible light irradiation. Faraday Discuss 215:313–328

Kumar A, Sadanandhan AM, Jain SL (2019) Silver doped reduced graphene oxide as a promising plasmonic photocatalyst for oxidative coupling of benzylamines under visible light irradiation. New J Chem 43(23):9116–9122

Lee KS, Shim J, Park M et al (2017) Transparent nanofiber textiles with intercalated ZnO@graphene QD LEDs for wearable electronics. Compos Part B Eng 130:70–75. https://doi.org/10.1016/j.compositesb.2017.07.046

Li J, Zhang X, Ai Z, Jia F, Zhang L, Lin J (2007) Efficient visible light degradation of rhodamine B by a photo-electrochemical process based on a Bi WO nanoplate film electrode. J Phys Chem C 111(18):6832–6836

Li L, Zhuang H, Bu D (2011) Characterization and activity of visible-light-driven TiO_2 photocatalyst codoped with lanthanum and iodine. Appl Surf Sci 257:9221–9225. https://doi.org/10.1016/j.apsusc.2011.06.007

Li J, Cui M, Guo Z et al (2015a) Preparation of p-n junction $BiVO_4$/Ag_2O heterogeneous nanostructures with enhanced visible-light photocatalytic activity. Mater Lett 151:75–78. https://doi.org/10.1016/j.matlet.2015.03.078

Li X, Yu J, Low J et al (2015b) Engineering heterogeneous semiconductors for solar water splitting. J Mater Chem A 3:2485–2534. https://doi.org/10.1039/c4ta04461d

Li J, Cui W, Sun Y et al (2017a) Directional electron delivery: via a vertical channel between g-C_3N_4 layers promotes photocatalytic efficiency. J Mater Chem A 5:9358–9364. https://doi.org/10.1039/c7ta02183f

Li X, Zhang H, Huang J et al (2017b) Folded nano-porous graphene-like carbon nitride with significantly improved visible-light photocatalytic activity for dye degradation. Ceram Int 43:15785–15792. https://doi.org/10.1016/j.ceramint.2017.08.144

Li Y, Li YL, Sa B, Ahuja R (2017c) Review of two-dimensional materials for photocatalytic water splitting from a theoretical perspective. Cat Sci Technol 7:545–559. https://doi.org/10.1039/c6cy02178f

Li S, Cai J, Wu X et al (2018a) TiO_2@Pt@CeO_2 nanocomposite as a bifunctional catalyst for enhancing photo-reduction of Cr (VI) and photo-oxidation of benzyl alcohol. J Hazard Mater 346:52–61. https://doi.org/10.1016/j.jhazmat.2017.12.001

Li Y, Ho W, Lv K et al (2018b) Carbon vacancy-induced enhancement of the visible light-driven photocatalytic oxidation of NO over g-C_3N_4 nanosheets. Appl Surf Sci 430:380–389. https://doi.org/10.1016/j.apsusc.2017.06.054

Li Z, Ma Q, Li Y et al (2018c) Flexible woven metal wires supported nanosheets and nanoparticles double-layered nitrogen-doped zinc stannate toward enhanced solar energy utilization. Ceram Int 44:905–914. https://doi.org/10.1016/j.ceramint.2017.10.021

Li R, Xie F, Liu J et al (2019a) Room-temperature hydrolysis fabrication of BiOBr/$Bi_{12}O_{17}Br_2$ Z-Scheme photocatalyst with enhanced resorcinol degradation and NO removal activity. Chemosphere 235:767–775. https://doi.org/10.1016/j.chemosphere.2019.06.231

Li S, Wang L, Li YD et al (2019b) Novel photocatalyst incorporating Ni-Co layered double hydroxides with P-doped CdS for enhancing photocatalytic activity towards hydrogen evolution. Appl Catal B Environ 254:145–155. https://doi.org/10.1016/j.apcatb.2019.05.001

Li X, Xiong J, Gao X et al (2019c) Recent advances in 3D g-C_3N_4 composite photocatalysts for photocatalytic water splitting, degradation of pollutants and CO_2 reduction. J Alloys Compd 802:196–209. https://doi.org/10.1016/j.jallcom.2019.06.185

Li X, Xiong J, Huang J et al (2019d) Novel g-C_3N_4/h′ZnTiO_3-a′TiO_2 direct Z-scheme heterojunction with significantly enhanced visible-light photocatalytic activity. J Alloys Compd 774:768–778. https://doi.org/10.1016/j.jallcom.2018.10.034

Li X, Xiong J, Xu Y et al (2019e) Defect-assisted surface modification enhances the visible light photocatalytic performance of g-C_3N_4@C-TiO_2 direct Z-scheme heterojunctions. Chin J Catal 40:424–433. https://doi.org/10.1016/S1872-2067(18)63183-3

Li Z, Song H, Guo R, Zuo M, Hou C, Sun S, He X, Sun Z, Chu W (2019f) Visible-light-induced condensation cyclization to synthesize benzimidazoles using fluorescein as a photocatalyst. Green Chem 21(13):3602–3605

Liu B, Xu B, Li S, Du J, Liu Z, Zhong W (2019) Heptazine-based porous graphitic carbon nitride: a visible-light driven photocatalyst for water splitting. J Mater Chem A 7(36):20799–20805

Low J, Yu J, Jaroniec M et al (2017) Heterojunction photocatalysts. Adv Mater 29:1–20. https://doi.org/10.1002/adma.201601694

Luque R, Balu AM (2013) Producing fuels and fine chemicals from biomass using nanomaterials. In: Producing fuels and fine chemicals from biomass using nanomaterials. SCITUS Academics LLC, New York, pp 1–315

Ma L, Fan H, Fu K et al (2017) Protonation of graphitic carbon nitride (g-C_3N_4) for an electrostatically self-assembling carbon@g-C_3N_4 core-shell nanostructure toward high hydrogen evolution. ACS Sustain Chem Eng 5:7093–7103. https://doi.org/10.1021/acssuschemeng.7b01312

Ma L, Wang G, Jiang C et al (2018) Synthesis of core-shell TiO_2@g-C_3N_4 hollow microspheres for efficient photocatalytic degradation of rhodamine B under visible light. Appl Surf Sci 430:263–272. https://doi.org/10.1016/j.apsusc.2017.07.282

Ma X, Luo M, Yan L, Tang N, Li J (2019) Preparation of a magnetically recyclable visible-light-driven photocatalyst based on phthalocyanine and its visible light catalytic degradation of methyl orange and -nitrophenol. New J Chem 43(24):9589–9595

Maeda K, Higashi M, Lu D, Abe R, Domen K (2010) Efficient nonsacrificial water splitting through two-step photoexcitation by visible light using a modified Oxynitride as a hydrogen evolution Photocatalyst. J Am Chem Soc 132(16):5858–5868

Malato S, Fernández-Ibáñez P, Maldonado MI et al (2009) Decontamination and disinfection of water by solar photocatalysis: recent overview and trends. Catal Today 147:1–59. https://doi.org/10.1016/j.cattod.2009.06.018

Meng Z, Oh W (2012) Photodegradation of organic dye by CoS_2 and carbon (C_{60}, graphene, CNT)/TiO_2 composite sensitizer. Chin J Catal 33:1495–1501. https://doi.org/10.1016/S1872-2067(11)60429-4

Meng P, Heng H, Sun Y, Liu X (2018) In situ polymerization synthesis of Z-scheme tungsten trioxide/polyimide photocatalyst with enhanced visible-light photocatalytic activity. Appl Surf Sci 428:1130–1140

Miao Y, Pan G, Huo Y, Li H (2013) Aerosol-spraying preparation of Bi_2MoO_6: a visible photocatalyst in hollow microspheres with a porous outer shell and enhanced activity. Dyes Pigments 99:382–389. https://doi.org/10.1016/j.dyepig.2013.05.005

Minero C, Pelizzetti E, Malato S, Blanco J (1996) Large solar plant photocatalytic water decontamination: effect of operational parameters. Solar Energy 56:421–428

Mohammadi M, Sabbaghi S (2014) Photo-catalytic degradation of 2,4-DCP wastewater using MWCNT/TiO_2 nano-composite activated by UV and solar light. Environ Nanotechnol Monit Manag 1–2:24–29. https://doi.org/10.1016/j.enmm.2014.09.002

Naseri A, Samadi M, Pourjavadi A et al (2017) Graphitic carbon nitride (g-C_3N_4)-based photocatalysts for solar hydrogen generation: recent advances and future development directions. J Mater Chem A 5:23406–23433. https://doi.org/10.1039/c7ta05131j

Nayak S, Mohapatra L, Parida K (2015) Visible light-driven novel g-C_3N_4/NiFe-LDH composite photocatalyst with enhanced photocatalytic activity towards water oxidation and reduction reaction. J Mater Chem A 3:18622–18635. https://doi.org/10.1039/c5ta05002b

Neil W, Ashcroft NDM (2016) Solid state physics. In: Facial plastic and reconstructive surgery. Thieme, New York, p 848

Niu Y, Xing M, Zhang J, Tian B (2013) Visible light activated sulfur and iron co-doped TiO_2 photocatalyst for the photocatalytic degradation of phenol. Catal Today 201:159–166. https://doi.org/10.1016/j.cattod.2012.04.035

Nuraje N, Asmatulu R, Kudaibergenov S (2012) Metal oxide-based functional materials for solar energy conversion: a review. Curr Inorg Chem 2:124–146. https://doi.org/10.2174/1877944111202020124

Nuraje N, Khan WS, Lei Y et al (2013) Superhydrophobic electrospun nanofibers. J Mater Chem A 1:1929–1946. https://doi.org/10.1039/c2ta00189f

Ohtani B (2010) Photocatalysis A to Z-what we know and what we do not know in a scientific sense. J Photochem Photobiol C: Photochem Rev 11:157–178. https://doi.org/10.1016/j.jphotochemrev.2011.02.001

Ong WJ, Tan LL, Ng YH et al (2016) Graphitic carbon nitride (g-C_3N_4)-based photocatalysts for artificial photosynthesis and environmental remediation: are we a step closer to achieving sustainability? Chem Rev 116:7159–7329. https://doi.org/10.1021/acs.chemrev.6b00075

Opoku F, Govender KK, van Sittert CGCE, Govender PP (2017) Recent progress in the development of semiconductor-based photocatalyst materials for applications in photocatalytic water splitting and degradation of pollutants. Adv Sustain Syst 1(7):1700006

Park JW, Kang M (2007) Synthesis and characterization of Ag_xO, and hydrogen production from methanol photodecomposition over the mixture of Ag_xO and TiO_2. Int J Hydrog Energy 32:4840–4846. https://doi.org/10.1016/j.ijhydene.2007.07.045

Qi K, Xie Y, Wang R et al (2019) Electroless plating Ni-P cocatalyst decorated g-C_3N_4 with enhanced photocatalytic water splitting for H_2 generation. Appl Surf Sci 466:847–853. https://doi.org/10.1016/j.apsusc.2018.10.037

Qin Y, Wang G, Wang Y (2007) Study on the photocatalytic property of La-doped CoO/$SrTiO_3$ for water decomposition to hydrogen. Catal Commun 8:926–930. https://doi.org/10.1016/j.catcom.2006.11.025

Ran J, Guo W, Wang H et al (2018a) Metal-free 2D/2D phosphorene/g-C_3N_4 van der waals heterojunction for highly enhanced visible-light photocatalytic H_2 production. Adv Mater 30:2–7. https://doi.org/10.1002/adma.201800128

Ran M, Li J, Cui W et al (2018b) Efficient and stable photocatalytic NO removal on C self-doped g-C_3N_4: electronic structure and reaction mechanism. Cat Sci Technol 8:3387–3394. https://doi.org/10.1039/c8cy00887f

Reddy DA, Kim EH, Gopannagari M et al (2019) Few layered black phosphorus/MoS_2 nanohybrid: a promising co-catalyst for solar driven hydrogen evolution. Appl Catal B Environ 241:491–498. https://doi.org/10.1016/j.apcatb.2018.09.055

Rengaraj S, Li XZ (2006) Enhanced photocatalytic activity of TiO_2 by doping with Ag for degradation of 2,4,6-trichlorophenol in aqueous suspension. J Mol Catal A Chem 243:60–67. https://doi.org/10.1016/j.molcata.2005.08.010

Rivera-Utrilla J, Sánchez-Polo M, Ferro-García MÁ, Prados-Joya G, Ocampo-Pérez R (2013) Pharmaceuticals as emerging contaminants and their removal from water: a review. Chemosphere 93(7):1268–1287

Rong X, Qiu F, Zhang C et al (2015) Preparation, characterization and photocatalytic application of TiO_2-graphene photocatalyst under visible light irradiation. Ceram Int 41:2502–2511. https://doi.org/10.1016/j.ceramint.2014.10.072

Sahoo DP, Patnaik S, Rath D, Mohapatra P, Mohanty A, Parida K (2019) Influence of Au/Pd alloy on an amine functionalised ZnCr LDH–MCM-41 nanocomposite: a visible light sensitive photocatalyst towards one-pot imine synthesis. Cat Sci Technol 9(10):2493–2513

Saliev T, Begimbetova D, Masoud AR, Matkarimov B (2019) Biological effects of non-ionizing electromagnetic fields: two sides of a coin. Prog Biophys Mol Biol 141:25–36. https://doi.org/10.1016/j.pbiomolbio.2018.07.009

Satsangi VR, Kumari S, Singh AP et al (2008) Nanostructured hematite for photoelectrochemical generation of hydrogen. Int J Hydrog Energy 33:312–318. https://doi.org/10.1016/j.ijhydene.2007.07.034

Sayama K, Yase K, Arakawa H, Asakura K, Tanaka A, Domen K (1998) Photocatalytic activity and reaction mechanism of Pt-intercalated $K_4Nb_6O_{17}$ catalyst on the water splitting in carbonate salt aqueous solution. J Photochem Photobiol A Chem 114:125–135

Sehati S, Entezari MH (2017) High visible light intercalated nanophotocatalyst (PbS-CdS/Ti6O13) synthesized by ultrasound: photocatalytic activity, photocorrosion resistance and degradation mechanism. Sep Purif Technol 174:482–492

Shakeel M, Arif M, Yasin G et al (2019) Layered by layered Ni-Mn-LDH/g-C_3N_4 nanohybrid for multi-purpose photo/electrocatalysis: morphology controlled strategy for effective charge carriers separation. Appl Catal B Environ 242:485–498. https://doi.org/10.1016/j.apcatb.2018.10.005

Shanker GS, Bhosale R, Ogale S, Nag A (2018) 2D nanocomposite of g-C_3N_4 and TiN embedded N-doped graphene for photoelectrochemical reduction of water using sunlight. Adv Mater Interfaces 5:1–8. https://doi.org/10.1002/admi.201801488

Shen R, Xie J, Zhang H et al (2018) Enhanced solar fuel H_2 generation over g-C_3N_4 nanosheet photocatalysts by the synergetic effect of noble metal-free Co_2P cocatalyst and the environmental phosphorylation strategy. ACS Sustain Chem Eng 6:816–826. https://doi.org/10.1021/acssuschemeng.7b03169

Shen G, Pu Y, Sun R, Shi Y, Cui Y, Jing P (2019) Enhanced visible light photocatalytic performance of a novel heterostructured Bi Ti O/BiOBr photocatalyst. New J Chem 43(33):12932–12940

Shi S, Gondal MA, Rashid SG, Qi Q, Al-Saadi AA, Yamani ZH, Sui Y, Xu Q, Shen K (2014) Synthesis of g-C3N4/BiOClxBr1−x hybrid photocatalysts and the photoactivity enhancement driven by visible light. Colloids Surf A Physicochem Eng Asp 461:202–211

Shi X, Fujitsuka M, Kim S, Majima T (2018) Faster electron injection and more active sites for efficient photocatalytic H_2 evolution in g-C_3N_4/MoS_2 hybrid. Small 14:1–9. https://doi.org/10.1002/smll.201703277

Shibata M, Kudo KA, Tanaka A et al (1987) Photocatalytic activities of layered titanium compounds and their derivatives for H_2 evolution from aqueous methanol solution. Chem Lett:1017–1018

Shimidzu T, Iyoda T, Koide Y (1985) An advanced visible- light- induced water reduction with Dye-sensitized semiconductor powder catalyst. J Am Chem Soc 107:35–41

Spasiano D, Del Pilar Prieto Rodriguez L, Olleros JC et al (2013) TiO_2/Cu(II) photocatalytic production of benzaldehyde from benzyl alcohol in solar pilot plant reactor. Appl Catal B Environ 136–137:56–63. https://doi.org/10.1016/j.apcatb.2013.01.055

Spasiano D, Marotta R, Malato S et al (2015) Solar photocatalysis: materials, reactors, some commercial, and pre-industrialized applications. A comprehensive approach. Appl Catal B Environ 170–171:90–123. https://doi.org/10.1016/j.apcatb.2014.12.050

Spinelli P, Ferry E, Van De Groep J et al (2012) Plasmonic light trapping in thin-film Si solar cells. J Opt 14. https://doi.org/10.1088/2040-8978/14/2/024002

Sun S, Liang S (2017) Recent advances in functional mesoporous graphitic carbon nitride (mp g-C_3N_4) polymers Shaodong. Nanoscale:1–33. https://doi.org/10.1039/b000000x

Sun W, Zhang S, Wang C et al (2007) Enhanced photocatalytic hydrogen evolution over $CaTi_{1-x}Zr_xO_3$ composites synthesized by polymerized complex method. Catal Lett 119:148–153. https://doi.org/10.1007/s10562-007-9212-8

Tada H, Jin Q, Nishijima H et al (2011) Titanium(IV) dioxide surface-modified with iron oxide as a visible light photocatalyst. Angew Chemie Int Ed 50:3501–3505. https://doi.org/10.1002/anie.201007869

Taherzadeh MJ, Lennartsson PR, Teichert O, Nordholm H (2013) Bioethanol production processes. In: Biofuels production, Wiley, Hoboken, pp 211–253

Takashima T, Moriyama N, Fujishiro Y, Osaki J, Takeuchi S, Ohtani B, Irie H (2019) Visible-light-induced water splitting on a hierarchically constructed Z-scheme photocatalyst composed of zinc rhodium oxide and bismuth vanadate. J Mater Chem A 7(17):10372–10378

Tan B, Ye X, Li Y et al (2018) Defective anatase TiO_{2-x} mesocrystal growth in situ on g-C_3N_4 nanosheets: construction of 3D/2D Z-scheme heterostructures for highly efficient visible-light photocatalysis. Chem A Eur J 24:13311–13321. https://doi.org/10.1002/chem.201802366

Tang L, Wang J, Liu X, Shu X, Zhang Z, Wang J (2019) Fabrication of Z-scheme photocatalyst, Er3+:Y3Al5O12@NiGa2O4-MWCNTs-WO3, and visible-light photocatalytic activity for degradation of organic pollutant with simultaneous hydrogen evolution. Renew Energy 138:474–488

Tanveer M, Tezcanli Guyer G (2013) Solar assisted photo degradation of wastewater by compound parabolic collectors: review of design and operational parameters. Renew Sust Energ Rev 24:534–543. https://doi.org/10.1016/j.rser.2013.03.053

Tian Y, Chang B, Lu J et al (2013) Hydrothermal synthesis of graphitic carbon nitride-Bi_2WO_6 heterojunctions with enhanced visible light photocatalytic activities. ACS Appl Mater Interfaces 5:7079–7085. https://doi.org/10.1021/am4013819

Verma LK, Sakhuja M, Son J et al (2011) Self-cleaning and antireflective packaging glass for solar modules. Renew Energy 36:2489–2493. https://doi.org/10.1016/j.renene.2011.02.017

Wang X, Maeda K, Thomas A, Takanabe K, Xin G, Carlsson JM, Domen K, Antonietti M (2008) A metal-free polymeric photocatalyst for hydrogen production from water under visible light. Nat Mater 8:76–80. https://doi.org/10.1038/NMAT2317

Wang W, Huang X, Wu S et al (2013) Preparation of p-n junction $Cu_2O/BiVO_4$ heterogeneous nanostructures with enhanced visible-light photocatalytic activity. Appl Catal B Environ 134–135:293–301. https://doi.org/10.1016/j.apcatb.2013.01.013

Wang Y, Wang H, Chen F et al (2017) Facile synthesis of oxygen doped carbon nitride hollow microsphere for photocatalysis. Appl Catal B Environ 206:417–425. https://doi.org/10.1016/j.apcatb.2017.01.041

Wang W, Li G, An T et al (2018) Photocatalytic hydrogen evolution and bacterial inactivation utilizing sonochemical-synthesized g-C_3N_4/red phosphorus hybrid nanosheets as a wide-spectral-responsive photocatalyst: the role of type I band alignment. Appl Catal B Environ 238:126–135. https://doi.org/10.1016/j.apcatb.2018.07.004

Wang L, Gao X, Cheng Y et al (2019a) TiO_2@MgAl-layered double hydroxide with enhanced photocatalytic activity towards degradation of gaseous toluene. J Photochem Photobiol A Chem 369:44–53. https://doi.org/10.1016/j.jphotochem.2018.10.004

Wang X, Xiang Y, Zhou B et al (2019b) Enhanced photocatalytic performance of Ag/TiO_2 nanohybrid sensitized by black phosphorus nanosheets in visible and near-infrared light. J Colloid Interface Sci 534:1–11. https://doi.org/10.1016/j.jcis.2018.09.013

Wang S, Teng Z, Xu Y et al (2020) Defect as the essential factor in engineering carbon-nitride-based visible-light-driven Z-scheme photocatalyst. Appl Catal B Environ 260:118145. https://doi.org/10.1016/j.apcatb.2019.118145

Wei F, Liu Y, Zhao H et al (2018a) Oxygen self-doped g-C_3N_4 with tunable electronic band structure for unprecedentedly enhanced photocatalytic performance. Nanoscale 10:4515–4522. https://doi.org/10.1039/c7nr09660g

Wei H, McMaster WA, Tan JZY et al (2018b) Tricomponent brookite/anatase TiO_2/g-C_3N_4 heterojunction in mesoporous hollow microspheres for enhanced visible-light photocatalysis. J Mater Chem A 6:7236–7245. https://doi.org/10.1039/c8ta00386f

Wei Y, Zhu Y, Jiang Y (2019) Photocatalytic self-cleaning carbon nitride nanotube intercalated reduced graphene oxide membranes for enhanced water purification. Chem Eng J 356:915–925

Wen J, Xie J, Chen X, Li X (2017) A review on g-C 3 N 4-based photocatalysts. Appl Surf Sci 391:72–123

Wu Y, Zhang J, Xiao L, Chen F (2010) Properties of carbon and iron modified TiO_2 photocatalyst synthesized at low temperature and photodegradation of acid orange 7 under visible light. Appl Surf Sci 256:4260–4268. https://doi.org/10.1016/j.apsusc.2010.02.012

Wu J, Huang S, Jin Z et al (2018) Black phosphorus: an efficient co-catalyst for charge separation and enhanced photocatalytic hydrogen evolution. J Mater Sci 53:16557–16566. https://doi.org/10.1007/s10853-018-2830-2

Wu H-Z, Liu J, Li L-L, Wang Z, Zhong Q-H, Bandaru S, Lau WM (2019) Exploring the formation and electronic structure properties of the g-C_3N_4 nanoribbon with density functional theory. J Phys Condens Matter 30:22

Xin Y, Huang Y, Lin K, Yu Y, Zhang B (2018) Self-template synthesis of double-layered porous nanotubes with spatially separated photoredox surfaces for efficient photocatalytic hydrogen production. Sci Bull 63(10):601–608

Xiong T, Cen W, Zhang Y, Dong F (2016) Bridging the g-C_3N_4 interlayers for enhanced photocatalysis. ACS Catal. https://doi.org/10.1021/acscatal.5b02922

Xue Y, Sun M (2019) Engineering hierarchical NiFe-layered double hydroxides derived phosphosulfide for high-efficiency hydrogen evolving electrocatalysis. Int J Hydrog Energy 44(31):16378–16386

Xu D, Cheng B, Cao S, Yu J (2015) Enhanced photocatalytic activity and stability of Z-scheme Ag_2CrO_4-GO composite photocatalysts for organic pollutant degradation. Appl Catal B Environ 164:380–388. https://doi.org/10.1016/j.apcatb.2014.09.051

Xu C, Qian L, Lin J et al (2019a) Heptazine-based porous polymer for selective CO_2 sorption and visible light photocatalytic oxidation of benzyl alcohol. Microporous Mesoporous Mater:9–14. https://doi.org/10.1016/j.micromeso.2019.03.011

Xu J, Fujitsuka M, Kim S et al (2019b) Unprecedented effect of CO_2 calcination atmosphere on photocatalytic H_2 production activity from water using g-C_3N_4 synthesized from triazole polymerization. Appl Catal B Environ 241:141–148. https://doi.org/10.1016/j.apcatb.2018.09.023

Xu X, Meng L, Dai Y et al (2020) Bi spheres SPR-coupled Cu_2O/Bi_2MoO_6 with hollow spheres forming Z-scheme Cu_2O/Bi/Bi_2MoO_6 heterostructure for simultaneous photocatalytic decontamination of sulfadiazine and Ni(II). J Hazard Mater 381:120953. https://doi.org/10.1016/j.jhazmat.2019.120953

Yanagida T, Sakata Y, Imamura H (2004) Photocatalytic decomposition of H_2O into H_2 and O_2 over Ga_2O_3 loaded with NiO. Chem Lett 33:726–727. https://doi.org/10.1246/cl.2004.726

Yang X, Chen Z, Xu J et al (2015) Tuning the morphology of g-C_3N_4 for improvement of Z-scheme photocatalytic water oxidation. ACS Appl Mater Interfaces 7:15285–15293. https://doi.org/10.1021/acsami.5b02649

Yang T, Peng J, Zheng Y, He X, Hou Y, Wu L, Fu X (2018) Enhanced photocatalytic ozonation degradation of organic pollutants by ZnO modified TiO2 nanocomposites. Appl Catal B Environ 221:223–234

Yang Y, Yan L, Li J et al (2019a) Synergistic adsorption and photocatalytic reduction of Cr (VI) using Zn-Al-layered double hydroxide and TiO_2 composites. Appl Surf Sci 492:487–496. https://doi.org/10.1016/j.apsusc.2019.06.229

Yang H, Wang J, Ma J, Yang H, Zhang J, Lv K, Wen L, Peng T (2019b) A novel BODIPY-based MOF photocatalyst for efficient visible-light-driven hydrogen evolution. J Mater Chem A 7(17):10439–10445

Yao G, Chen Z, Chen Q, Li D, Xie Z, Zhou Y, Xiong X, Xu Y (2018) Behaviors of organic and heavy metallic pollutants during supercritical water oxidation of oil-based drill cuttings. Water Air Soil Pollut 229(3)

Ye C, Li JX, Li ZJ et al (2015) Enhanced driving force and charge separation efficiency of protonated g-C_3N_4 for photocatalytic O_2 evolution. ACS Catal 5:6973–6979. https://doi.org/10.1021/acscatal.5b02185

Ye J, Liu J, Huang Z, Wu S, Dai X, Zhang L, Cui L (2019) Effect of reduced graphene oxide doping on photocatalytic reduction of Cr(VI) and photocatalytic oxidation of tetracycline by ZnAlTi layered double oxides under visible light. Chemosphere 227:505–513

Yeo CI, Kang EK, Lee SK, Song YM, Lee YT, Song YM, Lee YT (2014) Efficiency enhancement of III–V triple-junction solar cell using nanostructured bifunctional coverglass with enhanced transmittance and self-cleaning property. IEEE Photon J 6:1–9. https://doi.org/10.1109/JPHOT.2014.2319100

Yi XH, Ma SQ, Du XD et al (2019) The facile fabrication of 2D/3D Z-scheme g-C_3N_4/UiO-66 heterojunction with enhanced photocatalytic Cr(VI) reduction performance under white light. Chem Eng J:375. https://doi.org/10.1016/j.cej.2019.121944

Yu H, Shang L, Bian T et al (2016) Nitrogen-doped porous carbon nanosheets templated from g-C_3N_4as metal-free electrocatalysts for efficient oxygen reduction reaction. Adv Mater:5080–5086. https://doi.org/10.1002/adma.201600398

Yu K, Li X, Chen L, Fang J, Chen H, Li Q, Chi N, Ma J (2018) Mechanism and efficiency of contaminant reduction by hydrated electron in the sulfite/iodide/UV process. Water Res 129:357–364

Yuan Q, Liu Y, Le Li L et al (2009) Highly ordered mesoporous titania-zirconia photocatalyst for applications in degradation of rhodamine-B and hydrogen evolution. Microporous Mesoporous Mater 124:169–178. https://doi.org/10.1016/j.micromeso.2009.05.006

Zargazi M, Entezari MH (2018) BFO thin film on the stainless steel mesh by anodic EPD: a visible light photocatalyst for degradation of Rhodamin B. J Photochem Photobiol A Chem 365:185–198

Zargazi M, Entezari MH (2019a) Sonochemical versus hydrothermal synthesis of bismuth tungstate nanostructures: photocatalytic, sonocatalytic and sonophotocatalytic activities. Ultrason Sonochem 51:1–11

Zargazi M, Entezari MH (2019b) Anodic electrophoretic deposition of Bi2WO6 thin film: high photocatalytic activity for degradation of a binary mixture. Appl Catal B Environ 242:507–517

Zhang YC, Li J, Xu HY (2012) One-step in situ solvothermal synthesis of SnS_2/TiO_2 nanocomposites with high performance in visible light-driven photocatalytic reduction of aqueous Cr(VI). Appl Catal B Environ 123–124:18–26. https://doi.org/10.1016/j.apcatb.2012.04.018

Zhang AY, Wang WK, Pei DN, Yu HQ (2016) Degradation of refractory pollutants under solar light irradiation by a robust and self-protected ZnO/CdS/TiO_2 hybrid photocatalyst. Water Res 92:78–86. https://doi.org/10.1016/j.watres.2016.01.045

Zhang J, Qian H, Liu W et al (2018a) The construction of the heterostructural Bi_2O_3/g-C_3N_4 composites with an enhanced photocatalytic activity. Nano 13:1–9. https://doi.org/10.1142/S1793292018500637

Zhang L, Zhang Y, Huang S et al (2018b) Co_3O_4/Ni-based MOFs on carbon cloth for flexible alkaline battery-supercapacitor hybrid devices and near-infrared photocatalytic hydrogen evolution. Electrochim Acta 281:189–197. https://doi.org/10.1016/j.electacta.2018.05.162

Zhang W, Zhang Z, Choi SH, Yang W (2019) Facile enhancement of photocatalytic efficiency of g-C3N4 by Li-intercalation. Catal Today 321-322:67–73

Zhao H, Chen Y, Peng Q, Wang Q, Zhao G (2017) Catalytic activity of MOF(2Fe/Co)/carbon aerogel for improving H2O2 and OH generation in solar photo–electro–Fenton process. Appl Catal B Environ 203:127–137

Zhao S, Zhang Y, Zhou Y et al (2018) Facile one-step synthesis of hollow mesoporous g-C_3N_4 spheres with ultrathin nanosheets for photoredox water splitting. Carbon N Y 126:247–256. https://doi.org/10.1016/j.carbon.2017.10.033

Zhao H, Liu X, Dong Y, Li H, Song R, Xia Y, Wang H (2019) A novel visible-light-driven ternary Ag@Ag O/BiOCl Z-scheme photocatalyst with enhanced removal efficiency of RhB. New J Chem 43(35):13929–13937

Zheng Y, Yu Z, Ou H et al (2018) Black phosphorus and polymeric carbon nitride heterostructure for photoinduced molecular oxygen activation. Adv Funct Mater 28:1–9. https://doi.org/10.1002/adfm.201705407

Zhou S, Liu Y, Li J et al (2014) Facile in situ synthesis of graphitic carbon nitride (g-C_3N_4)-N-TiO_2 heterojunction as an efficient photocatalyst for the selective photoreduction of CO_2 to CO. Appl Catal B Environ 158–159:20–29. https://doi.org/10.1016/j.apcatb.2014.03.037

Zhu B, Xia P, Li Y et al (2017) Fabrication and photocatalytic activity enhanced mechanism of direct Z-scheme g-C_3N_4/Ag_2WO_4 photocatalyst. Appl Surf Sci 391:175–183. https://doi.org/10.1016/j.apsusc.2016.07.104

Zhu Y, Wang T, Xu T et al (2019) Size effect of Pt co-catalyst on photocatalytic efficiency of g-C_3N_4 for hydrogen evolution. Appl Surf Sci 464:36–42. https://doi.org/10.1016/j.apsusc.2018.09.061

Zong X, Sun C, Chen Z et al (2011) Nitrogen doping in ion-exchangeable layered tantalate towards visible-light induced water oxidation. Chem Commun 47:6293–6295. https://doi.org/10.1039/c0cc05440b